Dietary salt promotes neurovascular and cognitive dysfunction through a gut-initiated TH17 response

Giuseppe Faraco[1], David Brea[1], Lidia Garcia-Bonilla[1], Gang Wang[1], Gianfranco Racchumi[1], Haejoo Chang[1], Izaskun Buendia[1], Monica M. Santisteban[1], Steven G. Segarra[1], Kenzo Koizumi[1], Yukio Sugiyama[1], Michelle Murphy[1], Henning Voss [2], Joseph Anrather[1] and Costantino Iadecola[1]*

A diet rich in salt is linked to an increased risk of cerebrovascular diseases and dementia, but it remains unclear how dietary salt harms the brain. We report that, in mice, excess dietary salt suppresses resting cerebral blood flow and endothelial function, leading to cognitive impairment. The effect depends on expansion of TH17 cells in the small intestine, resulting in a marked increase in plasma interleukin-17 (IL-17). Circulating IL-17, in turn, promotes endothelial dysfunction and cognitive impairment by the Rho kinase–dependent inhibitory phosphorylation of endothelial nitric oxide synthase and reduced nitric oxide production in cerebral endothelial cells. The findings reveal a new gut–brain axis linking dietary habits to cognitive impairment through a gut-initiated adaptive immune response compromising brain function via circulating IL-17. Thus, the TH17 cell–IL-17 pathway is a putative target to counter the deleterious brain effects induced by dietary salt and other diseases associated with TH17 polarization.

A diet rich in sodium chloride (salt) is a well-established cause of morbidity and mortality worldwide[1]. Pioneering epidemiological studies across different populations first revealed a link between high salt intake, hypertension and cardiovascular diseases[2], but subsequent studies established that salt has also harmful effects independent of the elevation in blood pressure[3]. Based on this compelling evidence, health organizations issued recommendations to limit salt intake[4,5]. However, clinical trials did not unequivocally show a health benefit from these interventions, raising questions about the scientific evidence supporting indiscriminate salt curbing in the general population[6,7]. Consequently, there has been a long-standing controversy about the validity of restricting sodium intake and a call for additional research to gain a better understanding in its effects in health and disease[8].

The brain is a prime target of the harmful effects of salt, and a high salt diet (HSD) has been linked to cerebrovascular diseases and stroke, as well as cognitive impairment[9,10]. Systemic and cerebral blood vessels are profoundly affected by HSD. In particular, salt loading has been associated with failure of endothelial cells to modulate vascular tone, i.e., endothelial dysfunction, attributed to a deficit of the potent vasodilator nitric oxide (NO)[11,12]. However, it is not known how excess dietary salt leads to such NO deficit or whether the resulting vascular changes in the long run impair organ function. These unanswered questions are particularly relevant for the brain, an organ that relies critically on a continuous delivery of blood flow well matched to its dynamic energy needs[13]. Alterations in resting cerebral blood flow (CBF) and its regulation are well known to produce neuronal dysfunction and cognitive impairment[14] and could play a role in the harmful effects of excessive salt intake on the brain.

It has recently been reported that HSD leads to profound immune changes in the gut, resulting in increased susceptibility of the brain to autoimmunity. A diet rich in salt induces the accumulation in the gut of T-helper lymphocytes producing the proinflammatory cytokine interleukin-17 (TH17). The TH17 response is mediated by salt-induced activation of signaling pathways involving nuclear factor of activated T cell 5 (NFAT5) and serum glucocorticoid-regulated kinase 1 (SKG1), which, in turn, suppress the anti-inflammatory function of regulatory T cells, enabling TH17 polarization[15,16]. These changes in the gut have been shown to promote autoimmunity and exacerbate experimental allergic encephalomyelitis, an animal model of multiple sclerosis[15,16]. Considering that IL-17 is potentially vasotoxic[17,18], these observations raise the possibility that the TH17 response induced by dietary salt could play a role in the attendant vascular dysfunction.

We report that mice fed a high salt diet develop marked cerebral hypoperfusion and a profound alteration in the endothelial regulation of the cerebral microcirculation, leading to subsequent cognitive impairment. These effects depended on TH17 lymphocytes and were reproduced by recombinant IL-17 in mice fed a normal diet, pointing to their dependence on the HSD-induced TH17 response. The neurovascular and behavioral changes were mediated by suppression of endothelial NO by circulating IL-17, via Rho kinase (ROCK)-dependent inhibitory phosphorylation of endothelial NO synthase (eNOS). The findings unveil a gut–brain axis by which environmental factors linked to the diet lead to an adaptive immune response in the gut, promoting cerebral hypoperfusion, neurovascular dysregulation and cognitive impairment.

Results

HSD reduces resting cerebral blood flow and induces endothelial dysfunction, effects reversed by return to a normal diet. To examine the effects of dietary salt, we fed mice a HSD (4 or 8% NaCl), representing an 8-fold to 16-fold increase over the normal mouse diet. Although estimating salt consumption at the population level is challenging, this diet is comparable to the high end of the spectrum of human salt consumption[19]. Consistent with previous reports[20], HSD induced a nonsignificant trend toward a reduction

[1]Feil Family Brain and Mind Research Institute, Weill Cornell Medicine, New York, NY, USA. [2]Department of Radiology, Weill Cornell Medicine, New York, NY, USA. *e-mail: coi2001@med.cornell.edu

in body weight and increased caloric intake (Supplementary Fig. 1a), but did not increase arterial pressure (Fig. 1a and Supplementary Fig. 1b). Blood and urine analysis revealed no major metabolic alterations after 8–24 weeks of HSD, except for the anticipated increase in urine NaCl and reduction in creatinine, reflecting increased NaCl excretion, urinary dilution and increased urine output[21] (Supplementary Table 1).

To investigate the cerebrovascular effects of HSD, we examined resting CBF quantitatively using MRI with arterial spin labeling[22]. HSD induced a marked reduction in resting CBF both in cortex (−28%; $P < 0.05$; Fig. 1b) and hippocampus (−25%; $P < 0.05$; Supplementary Fig. 1d), which was fully developed at 8 weeks in cortex. Endothelial dysfunction was also observed in mice fed a 4% HSD for 12 weeks (Supplementary Fig. 1h). Since resting CBF is highly dependent on NO produced by eNOS[23], we examined whether HSD altered eNOS-dependent NO production and the associated cerebrovascular responses. Using laser-Doppler flowmetry in anesthetized mice equipped with a cranial window, we found that the local CBF increase produced by bathing the neocortex with acetylcholine (ACh), a response mediated by eNOS[23], was attenuated (−35%; Fig. 1c). Furthermore, resting NO production and the NO increase produced by ACh, assessed using DAF-FM, a NO-sensitive fluorescent dye, as a marker[24], was reduced in pial microvascular preparation from mice fed HSD (Fig. 1f and Supplementary Fig. 1i). The increases in somatosensory cortex CBF evoked by mechanical stimulation of the whiskers (functional hyperemia) was not reduced at 4 and 8 weeks of HSD ($P > 0.05$), but at 12 and 24 weeks, a tendency to attenuation was observed (Fig. 1d and Supplementary Fig. 1e,f). However, the reduction did not reach statistical significance, assessed both at the plateau of the CBF increase or as area under the curve (Fig. 1d and Supplementary Fig. 1e,f). Furthermore, the CBF response to neocortical application of the smooth muscle relaxant adenosine was not affected (Supplementary Fig. 1c). These observations indicate that HSD predominantly suppresses the endothelium-dependent response to ACh. The slight attenuation of functional hyperemia is consistent with impairment of the contribution of endothelial cells to the retrograde propagation of flow response triggered by neural activity[25].

Vascular inflammation has been linked to endothelial dysfunction[26]. However, we found no evidence of upregulation of inflammatory enzymes (NOX-2, MMPs or COX-2), adhesion molecules (ICAM, VCAM, etc.) or cytokines (IL-6, TNFα, etc.) in pial microvascular preparations of mice fed HSD for 12 weeks (Supplementary Fig. 2). Similarly, there was no upregulation of inflammatory genes in cerebral endothelial cells sorted from mice fed HSD (Supplementary Fig. 3a), suggesting that the neurovascular dysfunction was not due to a massive inflammatory response in cerebrovascular cells. Consistent with this conclusion, blood–brain barrier permeability, which is highly susceptible to cerebrovascular inflammation[14], was not altered in cortex or hippocampus of mice fed HSD (Supplementary Fig. 3b).

Next, we sought to determine whether the neurovascular effects of HSD are reversible by returning dietary salt intake to normal levels (NaCl 0.5%). To this end, after 12 weeks of HSD, mice were fed normal mouse chow for 4 weeks prior to examining cerebrovascular function. The normal diet restored both resting CBF and the reactivity of cerebral blood vessels to ACh, without altering mean arterial pressure (MAP; Fig. 1e and Supplementary Fig. 1g). These findings suggest that HSD impairs the ability of endothelial cells to produce NO, resulting in cerebral hypoperfusion and attenuation of endothelium-dependent responses, effects that can be reversed by returning to a normal diet.

HSD induces cognitive dysfunction. Normal cognition function requires an adequate, well-regulated delivery of blood flow[13]. Therefore, we investigated whether the neurovascular dysfunction

induced by HSD leads to cognitive impairment. To this end, we first used a novel object recognition task, which explores nonspatial memory[27]. HSD had no effect on the total time spent exploring the objects, but HSD mice spent equal time exploring novel and familiar objects, indicating a failure to identify the novel one. Of note, these deficits developed after 12 weeks of HSD (Fig. 2a), 8 weeks after the onset of neurovascular dysfunction. Return to normal diet was associated with normalization of the performance at the novel object recognition test (Fig. 2b). We also investigated the neurovascular and cognitive effect of HSD in middle-aged mice (age 14–16 months). Aging did not enhance the magnitude of the HSD-induced endothelial dysfunction, but it led to a significant attenuation of CBF response to whisker stimulation (Supplementary Fig. 4a), suggesting a worsening of the harmful cerebrovascular effects of HSD. Accordingly, in aged mice fed HSD, performance at the novel object task was impaired earlier (8 weeks; Supplementary Fig. 4b) than in young mice (12 weeks; Fig. 2a). Cognitive dysfunction was also observed at 12 weeks with a 4% HSD (Supplementary Fig. 1i).

To further investigate the effect of HSD on cognitive function we used the Barnes maze, a hippocampus-dependent task requiring spatial memory to learn and retain the location of an escape hole[28]. We found that mice fed either a normal diet or HSD learned to find the escape hole over the 3-day test, as indicated by the reduction in primary latency, distance traveled and errors made (Fig. 2c). However, when the escape hole was moved to the opposite quadrant, both primary latency and distance travelled were significantly longer on the last day of the test in mice fed HSD (Fig. 2c), indicating a deficit in spatial memory.

Lastly, we examined whether HSD affects nesting behavior. Nest building and burrowing are spontaneous rodent behaviors dependent on limbic function and akin to activities of daily living typically altered in patients with cognitive impairment[29]. The ability of the mice to build a nest, assessed by the Deacon rating scale[29], and the amount of nesting material used was reduced in HSD mice (Fig. 2d), attesting to disruption of this behavior. Therefore, HSD induces profound alterations in cognitive function that involve multiple domains, occur after the neurovascular dysfunction is fully developed and are reversible by normalization of salt intake.

The NO precursor L-arginine reverses the neurovascular and cognitive dysfunction of HSD. To provide further evidence implicating a deficit of NO in the effects of HSD, we administered the NO precursor L-arginine in the drinking water, starting at week 8 of the HSD and continuing until week 12, when cerebrovascular responses and cognition were tested. This approach has been used to increase production of endothelial NO and to rescue endothelial function[30]. L-Arginine did not affect MAP or resting vascular responses, but it completely reversed the cerebral endothelial dysfunction and cognitive deficits induced by HSD (Fig. 3a,b). The improvement of endothelial and cognitive function was associated with rescue of resting endothelial NO production and with an increase in NO produced by ACh, assessed in microvascular preparations (Fig. 3c and Supplementary Fig. 1i). These findings strengthen the association between the NO deficit and the neurovascular and cognitive dysfunction induced by HSD.

HSD increases inhibitory eNOS phosphorylation. The findings that HSD attenuates resting CBF, suppresses the increase in CBF induced by ACh and reduces endothelial NO production suggest that HSD may affect eNOS in brain endothelial cells. eNOS catalytic activity is dynamically regulated by phosphorylation. Thr^{495} phosphorylation reduces eNOS catalytic activity and NO production while Ser^{1177} phosphorylation increases them[31]. To determine whether HSD alters the phosphorylation state of eNOS, mice were fed HSD and then Thr^{495} and Ser^{1177} eNOS phosphorylation was
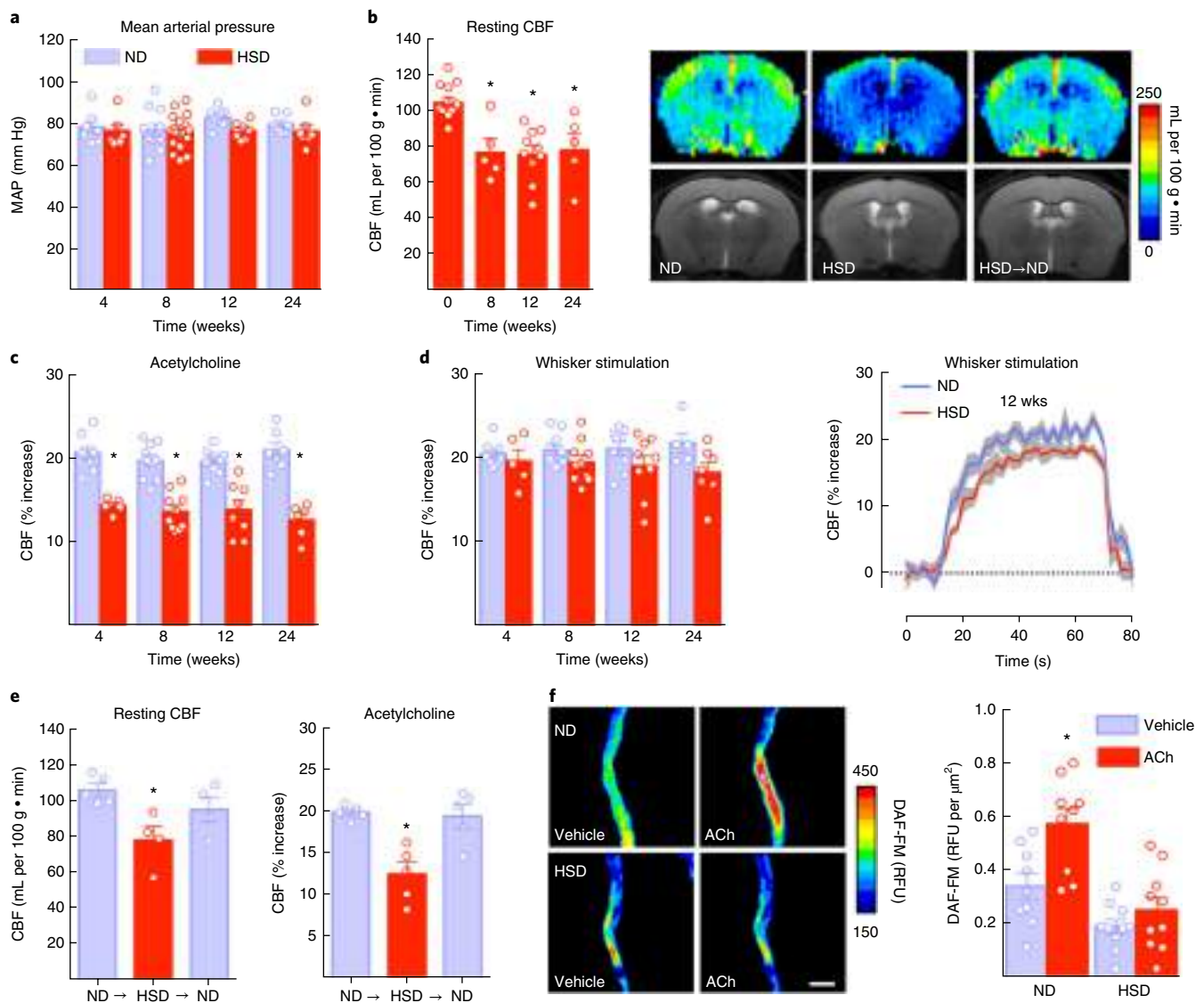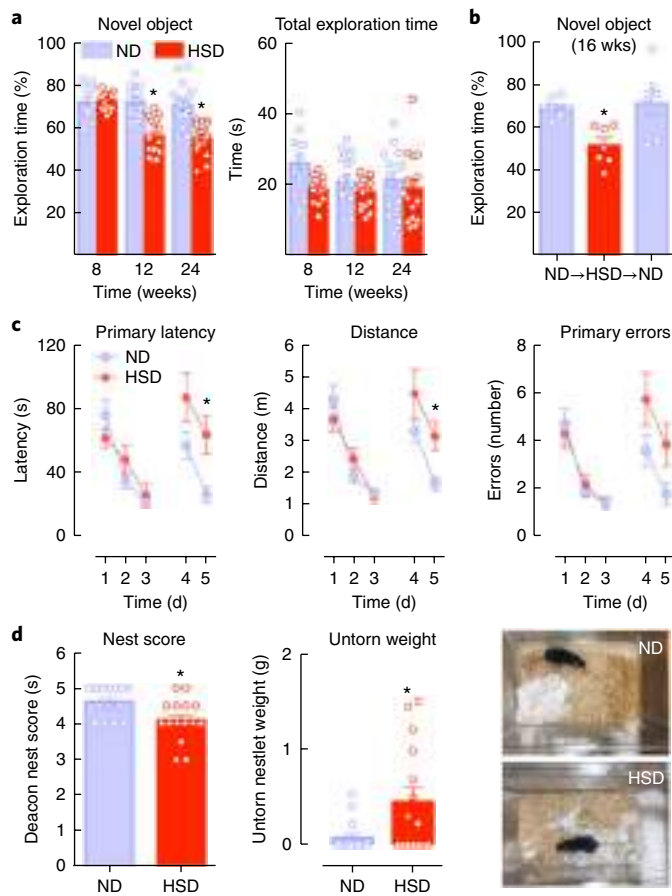
Fig. 1 | HSD reduces resting CBF and induces endothelial dysfunction, effects reversed by returning to a normal diet. a, HSD (NaCl 8%) does not alter MAP (diet: $P = 0.08134$, time: $P = 0.4982$; 4 weeks: normal diet (ND) and HSD, $n = 7$ and 6 mice, respectively; 8 weeks: ND and HSD $n = 11$ and 21 mice, respectively; 12 weeks: ND and HSD $n = 8$ and 9 mice, respectively; 24 weeks: ND and HSD $n = 7$ mice per group; two-way ANOVA and Tukey's test). **b**, HSD reduces resting CBF in the neocortex, assessed by arterial spin labeling MRI. The images show CBF after 12 weeks of HSD (*$P < 0.0001$; 0 weeks $n = 13$ mice, 8 weeks $n = 5$, 12 weeks $n = 10$, 24 weeks $n = 5$ mice per group; one-way ANOVA and Tukey's test). **c**, HSD attenuates the CBF increase induced by neocortical application of ACh (diet: *$P < 0.0001$, time: $P = 0.2858$; 4 weeks: ND and HSD $n = 8$ and 5 mice, respectively; 8 weeks: ND and HSD $n = 10$; 12 weeks: ND and HSD $n = 9$ and 8; 24 weeks: ND and HSD $n = 7$ and 6 mice per group; two-way ANOVA and Tukey's test). **d**, The CBF response to whisker stimulation shows a diet effect (diet: $P = 0.0066$, time: $P = 0.9966$), which did not reach statistical significance after Tukey's test (4 weeks: ND and HSD $n = 8$ and 5 mice, respectively; 8 weeks: ND and HSD $n = 10$ mice per group; 12 weeks: ND and HSD $n = 9$ mice per group; 24 weeks: ND and HSD $n = 5$ mice per group; two-way ANOVA and Tukey's test). Dotted line indicates the baseline CBF whereas the shaded area represents the standard error. **e**, The neurovascular effects of HSD (12 weeks) are reversible by returning dietary sodium intake to normal levels for 4 weeks (NaCl 0.5%; resting CBF: *$P < 0.0231$ vs. ND; ND $n = 5$, HSD and HSD→ND $n = 4$ mice per group; ACh: *$P = 0.0013$ vs. ND; ND, HSD and HSD→ND $n = 5$ mice per group; one-way ANOVA and Tukey's test). **f**, In isolated pial microvascular preparations, exposure to ACh (100 μM) increases NO production in mice fed ND, an effect attenuated in mice fed HSD for 12 weeks (diet: *$P = 0.0009$, treatment: *$P < 0.0001$; microvessels isolated from 9 ND and 10 HSD mice per group; repeated two-way ANOVA and Bonferroni's test). Scale bar, 50 μm. RFU, relative fluorescence unit. Data represent the average of 3 independent experiments. For all panels, data are expressed as mean ± s.e.m.

assessed in pial microvascular preparations. We found that HSD had no effect on Ser[1177] but increased eNOS phosphorylation at Thr[495] (Fig. 4a,b). Endothelin 1, a peptide implicated in the vascular effects of HSD[32], promotes eNOS inhibitory phosphorylation and attenuates ACh responses through endothelin type A (ET$_A$) receptors in cerebral arterioles[33]. However, the ET$_A$ receptor antagonist BQ123 failed to improve the CBF response to ACh (Supplementary Fig. 4c),

ruling out a role of endothelin 1 in the cerebrovascular effects of HSD. These findings indicate that the reduction in resting CBF and endothelial dysfunction are associated with inhibitory phosphorylation of eNOS and reduced production of endothelial NO.

HSD induces TH17 differentiation in the small intestine and increases IL-17 plasma levels. Since HSD promotes TH17

Fig. 2 | HSD induces delayed cognitive dysfunction. a, HSD induces deficits in recognition (nonspatial) memory as assessed by the novel object test, first observed after 12 weeks (diet: *$P < 0.0001$, time: *$P = 0.0046$; 8 weeks: ND and SD $n = 12$ and 15 mice, respectively; 12 weeks: ND and HSD $n = 15$ mice per group; 24 weeks: ND and HSD $n = 16$ mice per group; two-way ANOVA and Tukey's test). Total exploration time was not affected ($P > 0.05$). **b**, The deficit in novel object recognition is rescued by returning to normal diet for 4 weeks; *$P = 0.0137$ vs. ND; ND $n = 8$ mice; HSD and HSD→ND $n = 7$ mice per group; one-way ANOVA and Tukey's test). **c**, HSD (12 weeks) alters spatial memory, as assessed by the Barnes maze test. No differences in the latency to find the escape hole or distance traveled are observed during training (days 1–3). At days 4 and 5 latency and distance traveled are increased in the HSD group, suggesting a deficit in spatial memory (diet: *$P = 0.045$, time: *$P < 0.0001$; ND and HSD $n = 18$ and 15 mice, respectively; repeated-measures two-way ANOVA and Tukey's test). **d**, The ability to build a nest (nesting behavior), reflecting activities of daily living in rodents, is altered in mice fed HSD for 12 weeks, as indicated by a lower nest score (see Methods) and increased amount of untorn nesting material (nest score: *$P = 0.0267$ HSD vs. ND; untorn weight: *$P = 0.0254$ HSD vs. ND, $n = 15$ mice per group; two-tailed Mann–Whitney U test and two-tailed unpaired t test). Data are expressed as mean $\pm$ s.e.m.

Fig. 3 | The NO precursor L-arginine reverses the neurovascular and cognitive dysfunction of HSD. a, Administration of L-arginine in the drinking water (10 g per L), starting at week 8 of HSD and continued through week 12, did not alter MAP or CBF responses to whisker stimulation, but ameliorated the endothelial dysfunction induced by HSD (diet: *$P = 0.0043$; treatment: *$P = 0.0360$, ND vehicle (Veh) vs. L-arginine (L-arg) $n = 6$ and 5 mice per group, HSD Veh vs. L-arg $n = 6$ and 6 mice per group; two-way ANOVA and Tukey's test). **b**, The cognitive deficits induced by HSD were also improved by L-arginine administration (diet: =0.0366, treatment: *$P = 0.0118$; ND Veh vs. L-arg $n = 10$ mice per group, HSD Veh vs. L-arg $n = 12$ and 10 mice respectively; two-way ANOVA and Tukey's test). **c**, L-Arginine administration rescues the NO increase produced by ACh in cerebral microvascular preparations from HSD mice (diet: *$P = 0.0315$, treatment: *$P < 0.0001$; microvessels isolated from 5 ND and 6 HSD mice per group; repeated-measures two-way ANOVA and Bonferroni's test). Data are expressed as mean $\pm$ s.e.m.

differentiation in the small intestine[15,16], we investigated its effects on T-helper lymphocyte subtypes in gut, blood, brain and secondary lymphoid organs. Using IL-17 reporter mice carrying the gene encoding GFP at the endogenous *Il17a* locus[34], we found IL-17+ cells accumulating in the intestinal lamina propria of the distal small intestine (Fig. 5a,b). Flow-cytometric analysis of the lamina propria of the small intestine confirmed that the IL-17+ cells were TH17 lymphocytes (Fig. 5c,d), since IL-17+ γδ T cells, which also produce IL-17[34], were not increased (Fig. 5e). In agreement with previous observations in HSD[35], gut CD4+FoxP3+ regulatory
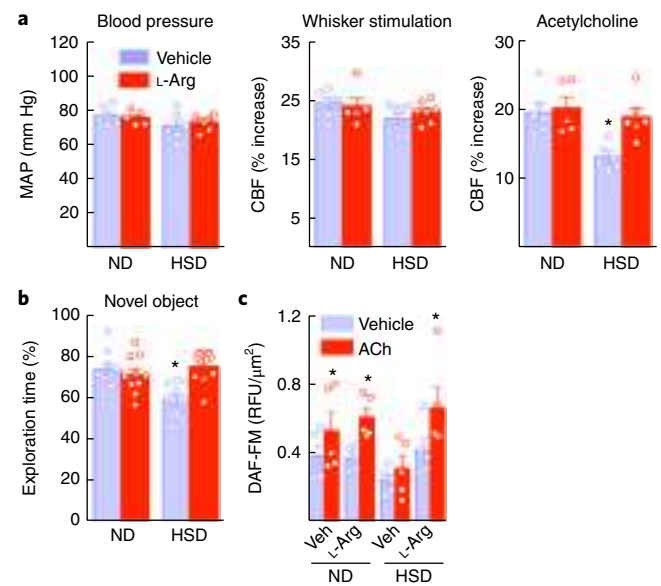
T cells were reduced and Th1 cells were not affected (Fig. 5f). A small increase in TH17 cells was also observed in lymph nodes and spleen, but not in blood (Fig. 5g). *Il17a* mRNA levels were also markedly increased in the distal small intestine, but not in cecum or colon (Fig. 5h and Supplementary Fig. 5b). No significant changes in IL-17-encoding mRNA were observed in blood, lymph nodes or spleen (Fig. 5i). Levels of mRNA for the IL-23 receptor, IL-22 and serum amyloid proteins, required for TH17 polarization, were also elevated (Supplementary Fig. 5a). TH17 cells and *Il17a* mRNA were not increased in brain or meninges, an important site of T cell accumulation in the CNS[36] (Supplementary Fig. 6a,c). HSD also increased plasma IL-17, which was first observed at 8 weeks and was still elevated at 24 weeks (Fig. 5j), whereas plasma TNFα and IL-6 were not increased (Supplementary Fig. 5c).Therefore, HSD induces the differentiation of TH17 cells predominantly in the distal small intestine leading to an increase in circulating IL-17.

The neurovascular and cognitive effects of HSD are not observed in mice lacking IL-17 or lymphocytes (*Rag1*−/− mice). Next, we investigated whether TH17 cells and IL-17 are involved in the neurovascular dysfunction and cognitive impairment induced by HSD. We first tested whether the effect depended on IL-17. To this end, *Il17a*−/− mice were fed HSD, and their cognitive function and CBF responses were tested. In these mice, gut *Il17a* mRNA and IL-17A plasma levels were below detection levels (Fig. 6a,b), and the attenuation in the response to ACh was ameliorated (Fig. 6c). These effects
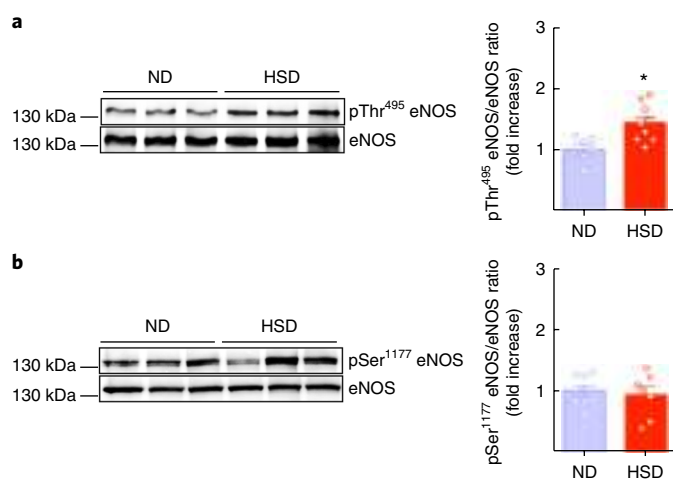
Fig. 4 | HSD increases inhibitory eNOS phosphorylation. a, HSD (8 weeks) increases the inhibitory phosphorylation of eNOS at Thr495 in isolated pial microvascular preparations (*$P = 0.0051$ vs. ND; microvessels isolated from 7 ND and 9 HSD mice per group; unpaired t test, two-tailed). **b**, The activatory phosphorylation of eNOS at Ser1177 is not affected by HSD ($P = 0.6615$ vs. ND; microvessels isolated from 8 ND and 7 HSD mice per group; unpaired t test, two-tailed). Data are derived from 2 independent experiments and expressed as mean ± s.e.m. Immunoblots in **a** and **b** are cropped; full gel pictures for immunoblots are shown in Supplementary Fig. 12.

were associated with normalization of eNOS inhibitory phosphorylation and improved performance at the novel object test (Fig. 6d,e). MAP or CBF responses to whisker stimulation and adenosine were not affected (Supplementary Fig. 7a). Brain perivascular macrophages are important mediators of neurovascular dysfunction[37], and high salt affects macrophage function[38]. However, depletion of brain macrophages with intracerebroventricular administration of clodronate, 1 week prior to termination of the HSD regimen (12 weeks), did not prevent the neurovascular dysfunction (Supplementary Fig. 8a,b), ruling out a role of these cells.

To provide further evidence that lymphocytes are the source of IL-17 we investigated lymphocyte-deficient *Rag1*−/− mice fed HSD. In these mice, HSD did not increase intestinal *Il17a* mRNA and IL-17 plasma levels (Fig. 6f,g), and the suppression of the CBF response to ACh, the increase in the inhibitory eNOS phosphorylation and the attendant cognitive impairment were not observed (Fig. 6h–j). MAP and CBF responses to whisker stimulation or adenosine were not altered (Supplementary Fig. 7b). These observations, in conjunction with the flow cytometry data showing selective upregulation of intestinal TH17 cells, implicate IL-17 production by TH17 lymphocytes in the neurovascular and cognitive dysfunction associated with HSD.

The neurovascular and the cognitive effects of HSD are prevented by IL-17-neutralizing antibodies and reproduced by recombinant IL-17 in mice fed a normal diet. To provide more direct evidence that IL-17 is responsible for the neurovascular and cognitive dysfunction of HSD, mice were treated with IL-17 neutralizing antibodies or isotype IgG control antibodies (100 μg per mouse every 3 d via intraperitoneal (i.p.) injection), starting at week 10 of HSD and continuing until the 12-week HSD treatment was completed. IL-17 antibodies did not affect MAP or functional hyperemia or the CBF response to adenosine (Supplementary Fig. 7c), but prevented the eNOS inhibitory phosphorylation and ameliorated the endothelial dysfunction and cognitive deficits induced by HSD (Fig. 7a–c). Conversely, in mice fed a normal diet,

systemic administration of exogenous IL-17 (1 μg per d for 7 d; i.p.) increased plasma IL-17 to the same level as HSD and reproduced the endothelial dysfunction, eNOS phosphorylation and cognitive dysfunction associated with HSD (Fig. 7d–f), independently of changes in MAP (Supplementary Fig. 7d). These data implicate circulating IL-17 as a key effector of the neurovascular and cognitive changes induced by HSD.

IL-17 induces ROCK-dependent increases in inhibitory eNOS phosphorylation and dampens endothelial NO production. The evidence presented above suggests that circulating IL-17, rather than circulating lymphocytes, acts on cerebral endothelial cells to induce eNOS inhibitory phosphorylation leading to reductions in NO production and brain hypoperfusion. Consistent with this suggestion, administration of FTY720 (1 mg per kg i.p., once every 3 d), a sphingosine-1-phosphate-receptor modulator that prevents lymphocyte egress from lymphoid organs[39], starting 2 weeks prior to the completion of the 12-week HSD treatment, reduced circulating T cells but did not prevent the neurovascular dysfunction (Supplementary Fig. 8c,d). To provide further evidence for an endothelial effect of circulating IL-17, we exposed mouse brain endothelial cells to IL-17 (1 and 10 ng per mL for 24 h) and assessed eNOS phosphorylation and NO production. IL-17-induced eNOS inhibitory phosphorylation associated with a reduction in baseline NO production and suppression of the increase in NO produced by ACh (Fig. 8a–c). The effect of IL-17 on the endothelium was not related to inflammation because, as in cerebral endothelial cells of mice exposed to HSD, IL-17 did not upregulate inflammatory genes (Supplementary Fig. 10). As a positive control, TNF-α induced a profound upregulation of inflammatory genes in these cells (Supplementary Fig. 10). ROCK is one of the major kinases implicated in inhibitory eNOS phosphorylation[40], and, consistent with its involvement in the effects of HSD, the ROCK inhibitor Y27632 (5 μM) prevented the IL-17-induced eNOS phosphorylation and attenuation of the NO increase induced by ACh (Fig. 8a–c). Inhibition of other kinases implicated in eNOS phosphorylation (PKC, Erk)[40,41] did not counteract the effect of IL-17 on ACh-induced NO production (Fig. 8c). ROCK-dependent eNOS inhibitory phosphorylation was also observed in human cerebral endothelial cells treated with IL-17, an effect first observed at a concentration (1 ng/mL) lower than that effective in mouse brain endothelial cells (10 ng/mL; Supplementary Fig. 9).

ROCK inhibition ameliorates the neurovascular and cognitive dysfunction of HSD. Finally, we asked whether administration of the ROCK inhibitor Y27632 would counteract the effects of HSD on neurovascular function and cognition. Treatment with Y27632 (10 mg per kg per d; i.p.) for the last 2 weeks of the 12-week HSD administration did not affect plasma IL-17 elevation or MAP, but prevented the eNOS phosphorylation, the attenuation of the CBF response to ACh and the behavioral dysfunction induced by HSD (Fig. 8d–h). CBF responses to whisker stimulation and adenosine were not affected (Supplementary Fig. 8e).

Discussion

We investigated the mechanisms of the harmful effects of dietary salt on the brain. It has long been known that HSD leads to alterations in endothelial function of cerebral and systemic vessels resulting from a reduction in endothelial NO[11]. However, most studies focused on salt-induced hypertension[8], and it has remained unclear how long-term dietary salt intake altered cerebrovascular regulation and brain function independently of blood pressure. Using a chronic model of HSD, mimicking sustained high salt intake in humans, we found a marked reduction in resting CBF in cortex and hippocampus, associated with a selective deficit in the endothelial regulation of CBF. The effect was related to suppression of eNOS catalytic activity due
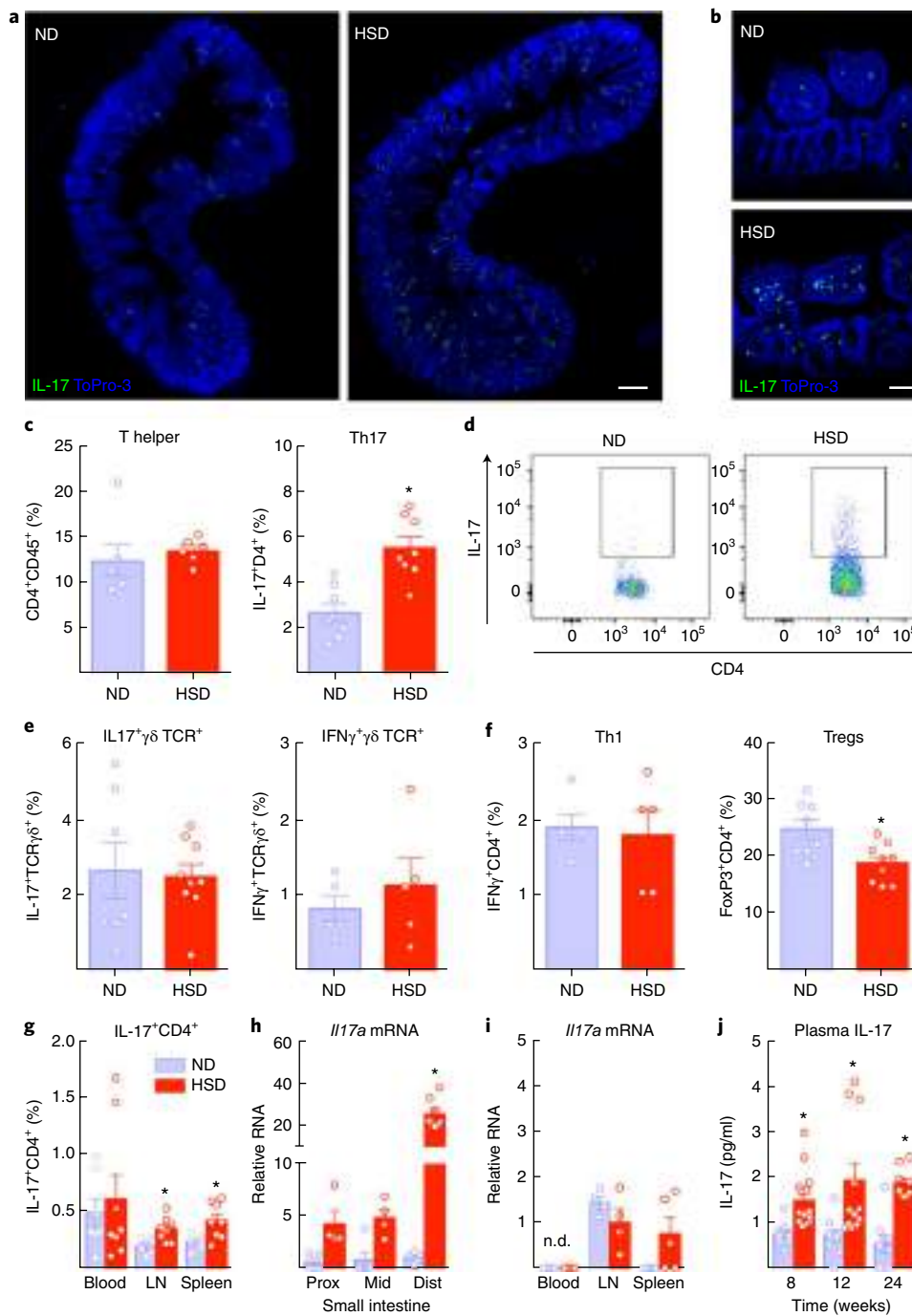
Fig. 5 | HSD induces TH17 differentiation in the small intestine and increases IL-17 plasma levels. a, IL-17^{+} cells accumulate in the lamina propria of the small intestine of IL-17-GFP reporter mice fed a HSD for 8 weeks (scale bar, 200 μm). **b**, Magnification showing localization of IL-17^{+}GFP^{+} cells to the lamina propria (scale bar, 50 μm). The experiment was repeated independently twice with similar results. **c**, HSD increases TH17 lymphocytes in the lamina propria (*$P = 0.0004$ vs. ND; $n = 8$ mice per group; unpaired t test, two-tailed), but T-helper lymphocytes are not increased ($P > 0.05$ vs. ND). **d**, Representative flow cytometry plot illustrating the increase in CD4^{+}IL-17^{+} cells (TH17) induced by HSD. The experiment was repeated independently twice with similar results. **e**, IL-17^{+} γδ T cells, another source of IL-17, or IFNγ[+] γδ T cells are not increased after HSD ($P = 0.8266$ and $P = 0.4446$ vs. ND; ND and HSD $n = 7$ and 9 mice per group (unpaired t test, two-tailed). Inset boxes indicate T-helper lymphocytes that are IL-17^{+}. **f**, Regulatory T cell (Treg) lymphocytes are reduced in the lamina propria of the small intestine of mice fed HSD, but TH1 cells are not affected (*$P = 0.0088$ vs. ND and $P = 0.7933$; $n = 8$ mice per group (unpaired t test, two-tailed). **g**, TH17 cells are slightly increased in lymph nodes and spleen (lymph nodes (LN): *$P = 0.0098$ vs. ND, ND and HSD $n = 6$ and 8 mice, respectively; spleen: *$P = 0.0061$, ND and HSD $n = 8$ mice per group, unpaired t test, two-tailed), but not in blood ($P > 0.05$ vs. ND). **h,i**, $Il17a$ mRNA, normalized to levels in the distal small intestine of ND mice, is markedly increased in the distal small intestine but is not increased in blood leukocytes, lymph nodes or spleen (diet: *$P < 0.0001$; proximal (prox) and middle (mid) small intestine: ND and HSD $n = 5$ and 4 mice, respectively; distal (dist) small intestine: ND and HSD $n = 6$ and 8 mice, respectively; blood: ND and HSD $n = 5$ mice per group; lymph nodes: ND and HSD $n = 4$ mice per group; spleen: ND and HSD $n = 5$ mice per group; two-way ANOVA and Tukey's test). **j**, HSD increases plasma IL-17 at 8, 12 and 24 weeks (diet: *$P < 0.0001$, time: $P = 0.2997$; 8 weeks: ND and HSD $n = 11$ and 15 mice, respectively; 12 weeks: ND and HSD $n = 10$ and 11 mice, respectively; 24 weeks: ND and HSD $n = 9$ mice per group; two-way ANOVA and Tukey's test). Data are expressed as mean ± s.e.m.
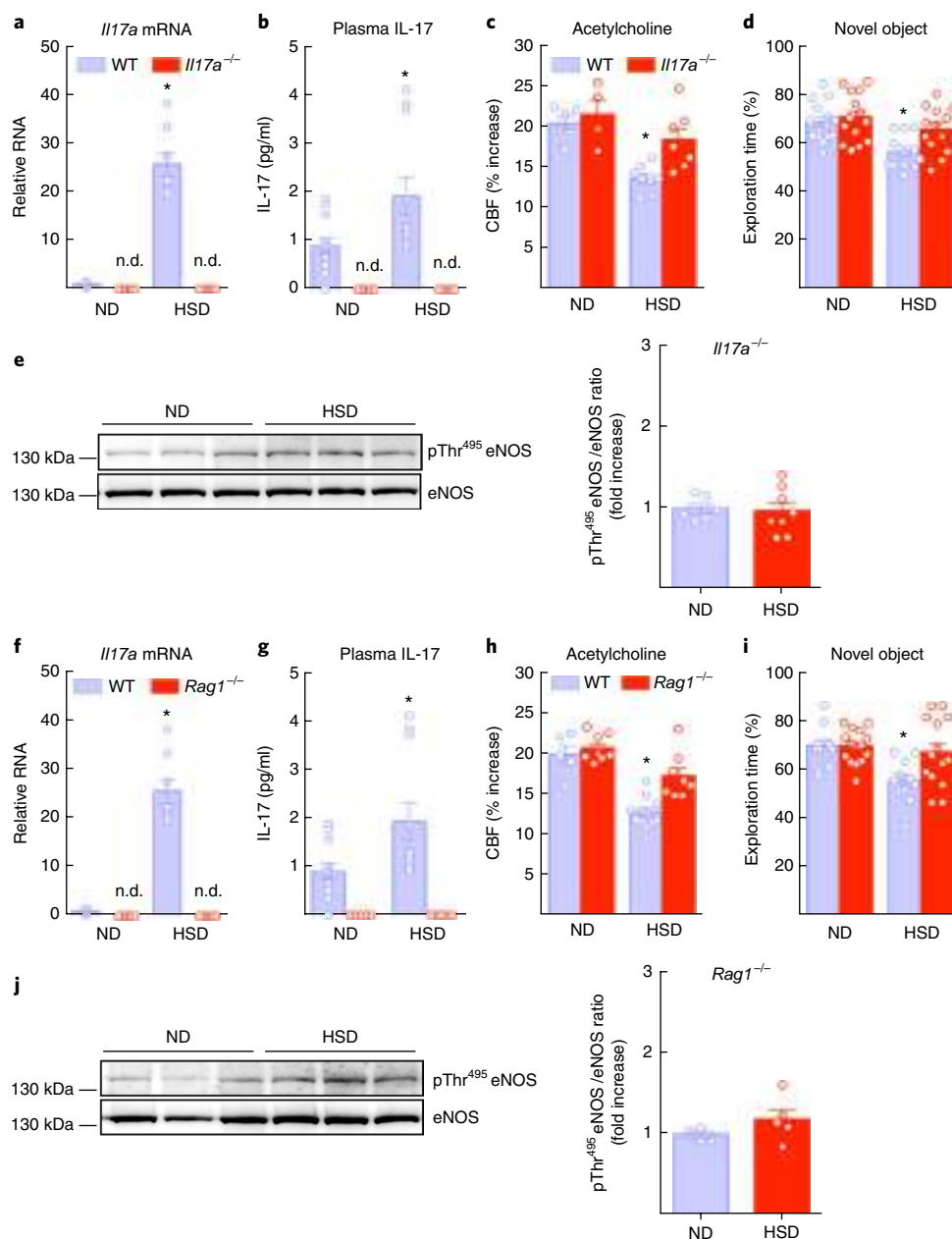
Fig. 6 | The neurovascular and cognitive effects of HSD are not observed in mice lacking IL-17 or lymphocytes (*Rag1*⁻/⁻ mice). a,b, *Il17a* mRNA in the distal small intestine and plasma IL-17 are not detectable (n.d.) in *Il17a*⁻/⁻ mice on HSD for 12 weeks (diet: *P < 0.0001, genotype: *P < 0.0001, mRNA: wild-type (WT) ND and HSD n = 6 and 8 mice, respectively, *Il17a*⁻/⁻ ND and HSD n = 5 mice per group; plasma: WT ND and HSD n = 12 and 10 mice per group, *Il17a*⁻/⁻ ND and HSD n = 5 mice per group; two-way ANOVA plus Tukey's test). **c,d**, The attenuation of the response to ACh and cognitive impairment induced by HSD are ameliorated in *Il17a*⁻/⁻ mice (ACh: diet: *P = 0.0003, genotype: *P = 0.0189; WT ND and HSD n = 6 and 8 mice, respectively, *Il17a*⁻/⁻ ND and HSD n = 4 and 7 mice per group; novel object recognition task (NOR): diet: *P = 0.0007, genotype: *P = 0.0202; WT ND and HSD n = 15 and 12 mice per group, *Il17a*⁻/⁻ ND and HSD n = 14 and 13 mice per group; two-way ANOVA and Tukey's test). **e**, eNOS inhibitory phosphorylation induced by HSD is not present in pial microvascular preparations of *Il17a*⁻/⁻ mice (P = 0.8043 vs. ND; microvessels from 6 ND and 8 HSD mice per group; unpaired *t* test, two-tailed). **f,g**, *Il17a* mRNA and plasma IL-17 are not detectable in *Rag1*⁻/⁻ mice on HSD for 12 weeks (diet: *P < 0.0001, genotype: *P < 0.0001, mRNA: WT ND and HSD n = 6 and 8 mice, respectivley, *Rag1*⁻/⁻ ND and HSD n = 5 mice per group; plasma: WT ND and HSD n = 12 and 10 mice, respectively, *Rag1*⁻/⁻ ND and HSD n = 5 mice per group; two-way ANOVA plus Tukey's test). **h,i**, The attenuation of the response to ACh and the attendant cognitive impairment induced by HSD are not observed in *Rag1*⁻/⁻ mice (ACh: diet: *P < 0.0001, genotype: *P = 0.0035; WT ND and HSD n = 5 and 10 mice, respectively, *Rag1*⁻/⁻ ND and HSD n = 8 mice per group; NOR: diet: *P = 0.0046, denotype: *P = 0.0496; WT ND and HSD n = 10 and 11 mice, respectively, *Rag1*⁻/⁻ ND and HSD n = 15 and 14 mice per group; two-way ANOVA and Tukey's test). **j**, HSD fails to increase eNOS inhibitory phosphorylation in *Rag1*⁻/⁻ mice (P = 0.2330 vs. ND; microvessels isolated from 4 ND and 5 HSD mice per group; unpaired *t* test, two-tailed). Data were obtained from 2 independent experiments and are expressed as mean ± s.e.m. Immunoblots in **e** and **j** are cropped; full gel pictures for immunoblots are shown in Supplementary Fig. 12.

to inhibitory eNOS phosphorylation and reduced NO production. These neurovascular alterations eventually led to cognitive impairment affecting different cognitive domains. The harmful effects of

HSD were abrogated by returning the mice to a normal diet, pointing to reversibility of the vascular dysfunction and cognitive impairment. Furthermore, the endothelial and cognitive dysfunction, as
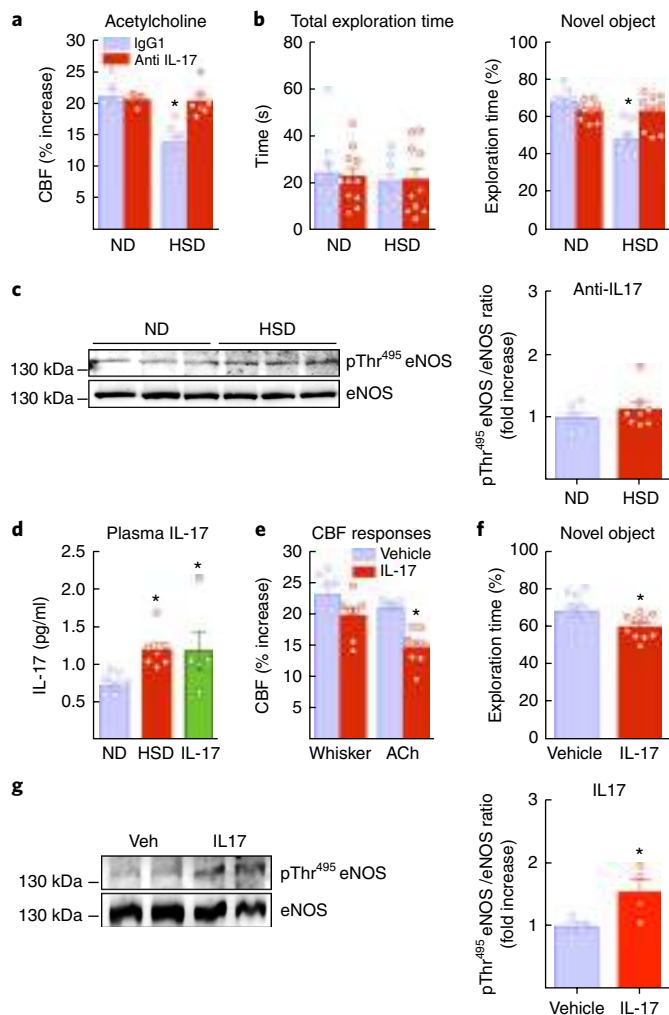
Fig. 7 | The neurovascular and the cognitive effects of HSD are prevented by IL-17-neutralizing antibodies and reproduced by IL-17 administration in mice fed a normal diet. a,b, Systemic (i.p.) administration of IL-17-neutralizing antibodies prevents the endothelial dysfunction and cognitive deficits of chronic (12 weeks) HSD (ACh: diet: *$P = 0.0013$, treatment: *$P = 0.0062$; ND IgG and anti-IL-17 $n = 6$ and 5 mice per group, HSD IgG and anti-IL-17 $n = 7$ mice per group; NOR: diet: *$P = 0.0003$, treatment: *$P = 0.0374$; ND IgG and anti-IL-17 $n = 10$ mice per group, HSD IgG and anti-IL-17 $n = 8$ and 10 mice per group; two-way ANOVA and Tukey's test). **c**, eNOS inhibitory phosphorylation is not increased in HSD mice injected with IL-17-neutralizing antibodies ($P = 0.3717$ vs. ND; microvessels isolated from 6 ND and 8 HSD mice per group; unpaired t test, two-tailed). **d**, Systemic administration of exogenous IL-17 (i.p.) for 1 week increases plasma IL-17 to the same level as HSD (*$P = 0.0137$ vs. ND; ND $n = 9$, HSD $n = 7$, IL-17 $n = 5$ mice per group; one-way ANOVA and Tukey's test). **e**, IL-17 and attenuates the CBF response to ACh (*$P = 0.003$ vs. Veh; Veh $n = 6$, IL-17 $n = 8$ mice per group; unpaired t test, two-tailed). **f**, IL-17 attenuates the performance at the novel object (*$P = 0.0422$ vs. Veh; Veh and IL-17 $n = 10$ mice per group; unpaired t test, two-tailed). **g**, IL-17 increases eNOS phosphorylation on Thr^{495} in cerebral blood vessels (*$P = 0.0473$ vs. ND; microvessels isolated from 4 Veh and IL-17 mice per group; unpaired t test, two-tailed). Data are expressed as mean ± s.e.m. Immunoblots in **c** and **g** are cropped; full gel pictures for immunoblots are shown in Supplementary Fig. 13.

well as the vascular NO deficit, were abrogated by treatment with the NO precursor L-arginine, providing further evidence for the involvement of endothelial NO in the cerebrovascular and cognitive effects of HSD. These observations unveil a previously undescribed

impact of HSD on resting cerebral perfusion, neurovascular regulation and cognitive function, independent of effects on arterial pressure and potentially reversible.

Since HSD leads to TH17 polarization in the small intestine, we tested the hypothesis that the cerebrovascular and cognitive effects of HSD were related to the attendant intestinal immune response. As anticipated, HSD induced TH17 expansion and IL-17 upregulation in the distal small intestine and in lymphoid organs, but not in brain or meninges. Notably, we found no evidence of cerebrovascular inflammation, ruling out the possibility that the vascular and cognitive effects may have been due to direct action of immune cells on the brain or blood vessels leading to a harmful inflammatory response. Rather, we observed a marked and sustained increase in circulating IL-17, a potentially vasotoxic cytokine[17,18]. Therefore, we explored the possibility that the deleterious vascular effects of HSD were caused by IL-17. Consistent with this hypothesis, we found that genetic deletion of IL-17 or systemic administration of IL-17-neutralizing antibodies prevented inhibitory eNOS phosphorylation, cerebrovascular dysfunction and cognitive deficits, whereas administration of recombinant IL-17 reproduced these effects in mice fed a normal diet. In vitro studies confirmed the harmful effects of IL-17 on endothelial function. Thus, exposure of mouse or human cerebral endothelial cells to IL-17 induced eNOS inhibitory phosphorylation and reduced the NO production evoked by ACh, effects prevented by inhibition of ROCK, a kinase responsible for eNOS inhibitory phosphorylation[40]. Finally, systemic administration of a ROCK inhibitor did not affect the elevation in plasma IL-17, but prevented eNOS phosphorylation, neurovascular dysfunction and cognitive deficits, attesting to the key role of this kinase in the vascular and cognitive effects of IL-17 in the setting of HSD. These findings, collectively, reveal a gut–brain axis whereby dietary salt induces cognitive impairment through adaptive immune changes initiated in the gut and leading to cerebrovascular endothelial dysfunction and cognitive deficits (Supplementary Fig. 11).

HSD induced a marked dysfunction of endothelial vasoactivity with reduced endothelial NO production and cognitive impairment. Endothelial dysfunction may lead to cognitive impairment by reducing resting CBF and altering microvascular flow distribution[42]. Accordingly, cerebral hypoperfusion and vascular dysregulation play a key role in cognitive impairment, both in animal models and in humans[43]. However, a unique feature of the neurovascular dysfunction induced by HSD is that it predominantly affects the endothelium. This is at variance with the cerebrovascular changes underlying cognitive impairment in models of amyloid pathology, inherited vasculopathies or hypertension[14,37], in which a more global alteration in cerebrovascular function is observed. In addition to its vascular effects, endothelial NO is also a potent neuromodulator, required for long-term potentiation and memory formation[42,44]. Although earlier studies attributed these effects to eNOS expression in neurons, later investigations confirmed the exclusive endothelial localization of this enzyme and implicated tonic NO production by endothelial cells in hippocampal long-term potentiation[44]. Therefore, eNOS dysfunction could also contribute to cognitive impairment by reducing baseline NO levels needed for normal hippocampal function.

IL-17 binds endothelial IL-17 receptors, leading to activation of signaling pathways involved in inflammation (NF-κB, MAPK, C/EBP)[45]. However, we did not observe evidence of vascular inflammation in mice fed HSD or in cerebral endothelial cells treated with IL-17, suggesting that the observed endothelial dysfunction was not a consequence of a nonspecific inflammatory response. Rather, the dysfunction was associated with inhibitory eNOS phosphorylation attributable to ROCK activation. In a model of hypertension induced by IL-17 administration, ROCK activation and inhibitory eNOS phosphorylation were also observed in the aorta[18], but the
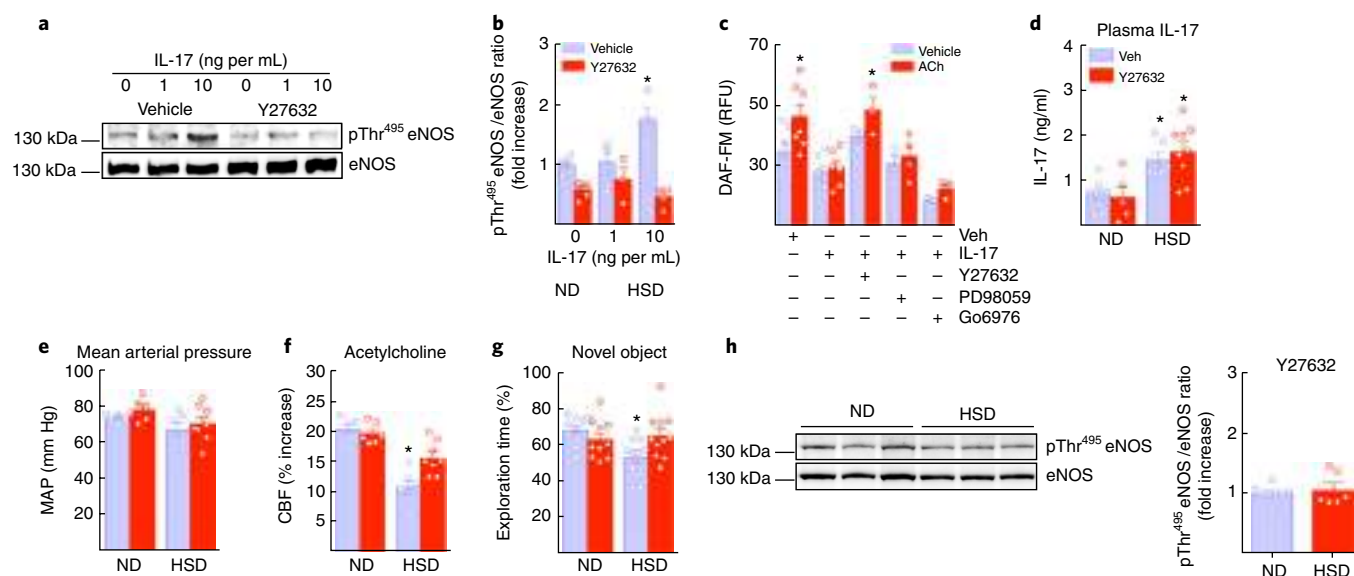
Fig. 8 | IL-17 suppresses NO production via ROCK, and ROCK inhibition ameliorates the neurovascular and cognitive dysfunction of HSD. a,b, IL-17 induces eNOS phosphorylation at Thr^{495} (*$P < 0.0001$ vs. vehicle 0 IL-17, $n = 3$–6 independent experiments; one-way ANOVA and Tukey's test). **c**, IL-17 attenuates the increase in NO induced by ACh in mouse brain endothelial cell cultures. The attenuation by IL-17 of the ACh-induced NO increase is prevented by coadministration of Y27632 (5 μM), but not by inhibitors of ERK (PD98059; 10 μM) or PKC (Go6976; 1 μM). NO increase: *$P = 0.0156$, treatment: *$P < 0.0001$; $n = 3$–6 independent experiments per group; repeated-measures two-way ANOVA and Tukey's test). **d**, Systemic administration of Y27632 does not affect the elevation in plasma IL-17 induced by 12 weeks of HSD (diet: *$P < 0.0001$, treatment: $P = 0.5559$, ND Veh and Y27632 $n = 9$ and 5 mice per group, HSD Veh and Y27632 $n = 7$ and 9 mice per group; two-way ANOVA and Tukey's test). **e**, MAP is also not affected (ND Veh and Y27632 $n = 6$ and 5 mice per group, HSD Veh and Y27632 $n = 6$ and 8 mice per /group). **f**, Y27632 prevents the attenuation of the CBF response to ACh induced by HSD (diet: *$P < 0.0001$, treatment: *$P = 0.0364$, ND Veh and Y27632 $n = 6$ mice per group, HSD Veh and Y27632 $n = 6$ and 8 mice per group; two-way ANOVA and Tukey's test). **g**, Y27632 prevents the behavioral dysfunction induced by HSD (diet: *$P = 0.0486$, ND Veh and Y27632 $n = 11$ and 10 mice per group, HSD Veh and Y27632 $n = 11$ and 11 mice per group; two-way ANOVA and Tukey's test). **h**, Y27632 blocks the increase in eNOS phosphorylation induced by HSD ($P = 0.5761$ vs. ND; microvessels isolated from 5 ND and 9 HSD mice per group; unpaired t test, two-tailed). Data were derived from 3 independent experiments and are expressed as mean ± s.e.m. Immunoblots in **a** and **h** are cropped; full gel pictures for immunoblots are shown in Supplementary Figs. 13 and 14.

signaling steps through which circulating IL-17 leads to endothelial ROCK activation remain to be defined. Irrespective of the mechanisms of ROCK activation by IL-17, the endothelial dysfunction and cognitive deficits induced by HSD are abrogated by ROCK inhibition despite the elevation in plasma IL-17, indicating that circulating IL-17 is unable to induce cognitive impairment in the absence of endothelial dysfunction. Thus, our data highlight the critical importance of cerebral endothelial function in cognitive health.

These data have implications that go beyond the pathology associated with HSD. Our findings suggest that the IL-17–ROCK pathway is a putative therapeutic target to counteract the deleterious cerebrovascular and cognitive effects of HSD and of other conditions associated with TH17 polarization. Activation of the TH17 cell–IL-17 pathway is observed in a number of diseases associated with cerebrovascular dysfunction, including, for example, multiple sclerosis, rheumatoid arthritis, psoriasis and inflammatory bowel disease[46–49]. Counteracting the deleterious effects of IL-17–ROCK on the cerebral endothelium would be beneficial to reduce cardiovascular risk in these conditions.

In conclusion, we have demonstrated that HSD induces a TH17 response in the gut that leads to increases in circulating IL-17, which, in turn, acts on cerebral endothelial cells to suppress endothelial NO production, leading to reductions in cerebral perfusion and cognitive dysfunction. While these findings highlight the key role of cerebral endothelial function in brain health, they also unveil a previously undescribed gut–brain axis whereby dietary habits compromise the brain microvasculature, leading to altered brain function and cognitive impairment.

Methods

Methods, including statements of data availability and any associated accession codes and references, are available at https://doi.org/10.1038/s41593-017-0059-z.

References

1. Mozaffarian, D. et al. Global sodium consumption and death from cardiovascular causes. *N. Engl. J. Med.* **371**, 624–634 (2014).
2. Zemel, M. B. & Sowers, J. R. Salt sensitivity and systemic hypertension in the elderly. *Am. J. Cardiol.* **61**, 7H–12H (1988).
3. Farquhar, W. B., Edwards, D. G., Jurkovitz, C. T. & Weintraub, W. S. Dietary sodium and health: more than just blood pressure. *J. Am. Coll. Cardiol.* **65**, 1042–1050 (2015).
4. Appel, L. J. et al. The importance of population-wide sodium reduction as a means to prevent cardiovascular disease and stroke: a call to action from the American Heart Association. *Circulation* **123**, 1138–1143 (2011).
5. Institute of Medicine (US) Committee on Strategies to Reduce Sodium Intake. *Strategies to Reduce Sodium Intake in the United States.* (Henney, J.E., Taylor, C.L. & Boon, C.S. eds.) (National Academies Press, Washington DC, 2010).
6. Kotchen, T. A., Cowley, A. W. Jr. & Frohlich, E. D. Salt in health and disease—a delicate balance. *N. Engl. J. Med.* **368**, 1229–1237 (2013).
7. Nicholls, M. G. Population-wide dietary sodium restriction: a cautious view. *Curr. Hypertens. Rep.* **13**, 325–327 (2011).
8. Oh, Y. S. et al. National Heart, Lung, and Blood Institute Working Group report on salt in human health and sickness: building on the current scientific evidence. *Hypertension* **68**, 281–288 (2016).
9. Heye, A. K. et al. Blood pressure and sodium: association with MRI markers in cerebral small vessel disease. *J. Cereb. Blood Flow. Metab.* **36**, 264–274 (2016).

10. Strazzullo, P., D'Elia, L., Kandala, N.-B. & Cappuccio, F. P. Salt intake, stroke, and cardiovascular disease: meta-analysis of prospective studies. *Br. Med. J.* **339**, b4567 (2009).

11. Boegehold, M. A. The effect of high salt intake on endothelial function: reduced vascular nitric oxide in the absence of hypertension. *J. Vasc. Res.* **50**, 458–467 (2013).

12. Cosic, A. et al. Attenuated flow-induced dilatation of middle cerebral arteries is related to increased vascular oxidative stress in rats on a short-term high salt diet. *J. Physiol. (Lond.)* **594**, 4917–4931 (2016).

13. Iadecola, C. The neurovascular unit coming of age: a journey through neurovascular coupling in health and disease. *Neuron* **96**, 17–42 (2017).

14. Iadecola, C. The pathobiology of vascular dementia. *Neuron* **80**, 844–866 (2013).

15. Kleinewietfeld, M. et al. Sodium chloride drives autoimmune disease by the induction of pathogenic TH17 cells. *Nature* **496**, 518–522 (2013).

16. Wu, C. et al. Induction of pathogenic TH17 cells by inducible salt-sensing kinase SGK1. *Nature* **496**, 513–517 (2013).

17. Kebir, H. et al. Human TH17 lymphocytes promote blood-brain barrier disruption and central nervous system inflammation. *Nat. Med.* **13**, 1173–1175 (2007).

18. Nguyen, H. et al. Interleukin-17 causes Rho-kinase-mediated endothelial dysfunction and hypertension. *Cardiovasc. Res.* **97**, 696–704 (2013).

19. Powles, J. et al. Global, regional and national sodium intakes in 1990 and 2010: a systematic analysis of 24 h urinary sodium excretion and dietary surveys worldwide. *BMJ Open.* **3**, e003733 (2013).

20. Cochet, H. et al. Comprehensive phenotyping of salt-induced hypertensive heart disease in living mice using cardiac magnetic resonance. *Eur. Radiol.* **23**, 332–338 (2013).

21. Schlote, J. et al. Cardiovascular and renal effects of high salt diet in GDNF+/- mice with low nephron number. *Kidney Blood Press. Res.* **37**, 379–391 (2013).

22. Jackman, K. A. et al. Dichotomous effects of chronic intermittent hypoxia on focal cerebral ischemic injury. *Stroke* **45**, 1460–1467 (2014).

23. Toda, N., Ayajiki, K. & Okamura, T. Cerebral blood flow regulation by nitric oxide: recent advances. *Pharmacol. Rev.* **61**, 62–97 (2009).

24. Wang, G. et al. Angiotensin II slow-pressor hypertension enhances NMDA currents and NOX2-dependent superoxide production in hypothalamic paraventricular neurons. *Am. J. Physiol. Regul. Integr. Comp. Physiol.* **304**, R1096–R1106 (2013).

25. Chen, B. R., Kozberg, M. G., Bouchard, M. B., Shaik, M. A. & Hillman, E. M. C. A critical role for the vascular endothelium in functional neurovascular coupling in the brain. *J. Am. Heart Assoc.* **3**, e000787 (2014).

26. Poggesi, A., Pasi, M., Pescini, F., Pantoni, L. & Inzitari, D. Circulating biologic markers of endothelial dysfunction in cerebral small vessel disease: a review. *J. Cereb. Blood Flow. Metab.* **36**, 72–94 (2016).

27. Cohen, S. J. et al. The rodent hippocampus is essential for nonspatial object memory. *Curr. Biol.* **23**, 1685–1690 (2013).

28. Barnes, C. A. Memory deficits associated with senescence: a neurophysiological and behavioral study in the rat. *J. Comp. Physiol. Psychol.* **93**, 74–104 (1979).

29. Deacon, R. M. Assessing nest building in mice. *Nat. Protoc.* **1**, 1117–1119 (2006).

30. Rosenblum, W. I., Nelson, G. H. & Shimizu, T. L-Arginine suffusion restores response to acetylcholine in brain arterioles with damaged endothelium. *Am. J. Physiol.* **262**, H961–H964 (1992).

31. Harris, M. B. et al. Reciprocal phosphorylation and regulation of endothelial nitric-oxide synthase in response to bradykinin stimulation. *J. Biol. Chem.* **276**, 16587–16591 (2001).

32. Smith, L., Payne, J. A., Sedeek, M. H., Granger, J. P. & Khalil, R. A. Endothelin-induced increases in Ca2+ entry mechanisms of vascular contraction are enhanced during high-salt diet. *Hypertension* **41**, 787–793 (2003).

33. Faraco, G. et al. Circulating endothelin-1 alters critical mechanisms regulating cerebral microcirculation. *Hypertension* **62**, 759–766 (2013).

34. Benakis, C. et al. Commensal microbiota affects ischemic stroke outcome by regulating intestinal γδ T cells. *Nat. Med.* **22**, 516–523 (2016).

35. Hernandez, A. L. et al. Sodium chloride inhibits the suppressive function of FOXP3+ regulatory T cells. *J. Clin. Invest.* **125**, 4212–4222 (2015).

36. Kipnis, J. Multifaceted interactions between adaptive immunity and the central nervous system. *Science* **353**, 766–771 (2016).

37. Faraco, G. et al. Perivascular macrophages mediate the neurovascular and cognitive dysfunction associated with hypertension. *J. Clin. Invest.* **126**, 4674–4689 (2016).

38. Binger, K. J. et al. High salt reduces the activation of IL-4- and IL-13-stimulated macrophages. *J. Clin. Invest.* **125**, 4223–4238 (2015).

39. Mandala, S. et al. Alteration of lymphocyte trafficking by sphingosine-1-phosphate receptor agonists. *Science* **296**, 346–349 (2002).

40. Sugimoto, M. et al. Rho-kinase phosphorylates eNOS at threonine 495 in endothelial cells. *Biochem. Biophys. Res. Commun.* **361**, 462–467 (2007).

41. Guterbaum, T. J. et al. Endothelial nitric oxide synthase phosphorylation at Threonine 495 and mitochondrial reactive oxygen species formation in response to a high H_2O_2 concentration. *J. Vasc. Res.* **50**, 410–420 (2013).

42. Katusic, Z. S. & Austin, S. A. Endothelial nitric oxide: protector of a healthy mind. *Eur. Heart J.* **35**, 888–894 (2014).

43. Love, S. & Miners, J. S. Cerebral hypoperfusion and the energy deficit in Alzheimer's disease. *Brain Pathol.* **26**, 607–617 (2016).

44. Garthwaite, J. Concepts of neural nitric oxide-mediated transmission. *Eur. J. Neurosci.* **27**, 2783–2802 (2008).

45. Gu, C., Wu, L. & Li, X. IL-17 family: cytokines, receptors and signaling. *Cytokine* **64**, 477–485 (2013).

46. Tablazon, I. L. D., Al-Dabagh, A., Davis, S. A. & Feldman, S. R. Risk of cardiovascular disorders in psoriasis patients: current and future. *Am. J. Clin. Dermatol.* **14**, 1–7 (2013).

47. Liou, T.-H. et al. Risk of stroke in patients with rheumatism: a nationwide longitudinal population-based study. *Sci. Rep.* **4**, 5110 (2014).

48. Ferro, J. M., Oliveira, S. N. & Correia, L. Neurologic manifestations of inflammatory bowel diseases. *Handb. Clin. Neurol.* **120**, 595–605 (2014).

49. Marshall, O. et al. Impaired cerebrovascular reactivity in multiple sclerosis. *JAMA Neurol.* **71**, 1275–1281 (2014).

Author contributions

Study design: C.I., J.A. and G.F. Conducting experiments and acquiring data: G.F., D.B., L.G.B., G.W., G.R., H.C., I.B., M.M.S., S.G.S., K.K., Y.S., M.M. and H.V. Analyzing data: G.F., D.B., G.W., H.C., I.B., M.M.S. and K.K. Writing the manuscript: G.F. and C.I.

Competing interests

The authors declare no competing financial interests.

Additional information

Supplementary information is available for this paper at https://doi.org/10.1038/s41593-017-0059-z.

Reprints and permissions information is available at www.nature.com/reprints.

Correspondence and requests for materials should be addressed to C.I.

Publisher's note: Springer Nature remains neutral with regard to jurisdictional claims in published maps and institutional affiliations.

Methods

Mice. All procedures were approved by the institutional animal care and use committee of Weill Cornell Medicine (Animal protocol number: 0807-777A). Studies were conducted according to the ARRIVE guidelines (https://www.nc3rs.org.uk/arrive-guidelines), in the following lines of male mice: C57BL/6 (JAX), B6.129S7-Rag1tm1Mom/J (*Rag1*−/−, JAX Stock #002216), IL-17atm1.1(icre)Stck/J (*Il17a*−/−, JAX Stock #016869) and C57BL/6-IL-17atm1Bcgen/J (IL-17GFP, JAX Stock #018472). See also the Life Sciences Reporting Summary for additional details.

High salt diet. Mice (8 weeks old) received normal chow (0.5% NaCl) and tap water ad libitum (normal diet) or sodium-rich chow (4% or 8% NaCl) and tap water containing 1% NaCl ad libitum (HSD) for 4 to 24 weeks according to the experiment. We used 12- to13-month-old C57BL/6 male mice in the experiments aimed at evaluating the interaction between aging and HSD.

In vivo treatments. L-Arginine (10 g/L; Sigma) was administered in the drinking water starting at week 8 of HSD and continuing until week 12. Normal and HSD mice were treated (every three days; i.p.) with 100 μg/mouse of anti-IL-17A (Clone 17F3; bioXcell) or mouse IgG1 isotype control (Clone MOPC-21; bioXcell) antibodies for the last two weeks of the HSD treatment period (12 weeks) prior to behavioral and cerebrovascular studies. The same length and timing of administration were used in the experiments with Rho-kinase inhibitor Y27632 (10 mg/kg; Tocris). FTY720 (1 mg/kg; Cayman Chemical) was injected i.p. three times every 3 d during the last two weeks of the HSD treatment period (12 weeks) and CBF studies. Clodronate was injected i.c.v. as previously described[37] 1 week prior to termination of the 12-week HSD treatment period. rIL-17A (1 μg/d; Peprotech) or vehicle was administered i.p. for 1 week in mice fed ND, and CBF response and behavior were assessed.

General surgical procedures for CBF studies. Mice were anesthetized with isoflurane (induction, 5%; maintenance, 2%)[37]. The trachea was intubated and mice were artificially ventilated with a mixture of N_2 and O_2. One of the femoral arteries was cannulated for recording mean arterial pressure (MAP) and collecting blood samples. Rectal temperature was maintained at 37 °C. End tidal CO_2, monitored by a CO_2 analyzer (Capstar-100, CWE Inc.), was maintained at 2.6–2.7% to provide a pCO_2 of 30–40 mmHg and a pH of 7.3–7.4[37]. After surgery, isoflurane was discontinued and anesthesia was maintained with urethane (750 mg/kg, i.p.) and chloralose (50 mg/kg, i.p.). Throughout the experiment, the level of anesthesia was monitored by testing motor responses to tail pinch.

Monitoring cerebral blood flow. A small craniotomy (2 × 2 mm) was performed to expose the parietal cortex, the dura was removed and the site was superfused with Ringer's solution (37 °C; pH 7.3–7.4)[37]. CBF was continuously monitored at the site of superfusion with a laser-Doppler probe (Perimed) positioned stereotaxically ~0.5 mm above the cortical surface and connected to a data acquisition system (PowerLab). CBF values were expressed as percentage increases relative to the resting level[33].

Protocol for CBF experiments. After MAP and blood gases were stable, CBF responses were recorded. To minimize the confounding effects of anesthesia on vascular reactivity, the time interval between the administration of urethane-chloralose and the testing of CBF responses was kept consistent among the different groups of mice studied[33]. The whisker-barrel cortex was activated for 60 s by stroking the contralateral vibrissae, and the evoked changes in CBF were recorded. We recorded CBF in the regions of the somatosensory cortex exhibiting the maximal increases in CBF, as verified by mapping the cortical surface at different sites. The whiskers were activated until the CBF signal reached a stable plateau. The endothelium-dependent vasodilator acetylcholine (ACh; 10 μM; Sigma), or the smooth muscle relaxant adenosine (400 μM; Sigma) were superfused on the exposed neocortex for 5 min, and the associated CBF changes were recorded[37].

Measurement of resting CBF by ASL-MRI. CBF was assessed quantitatively using arterial spin labeling magnetic resonance imaging (ASL-MRI), performed on a 7.0-tesla 70/30 Bruker Biospec small-animal MRI system with 450 mT/m gradient amplitude and a 4,500 T · m−1 · s−1 slew rate[22]. A volume coil was used for transmission and a surface coil for reception. Anatomical localizer images were acquired to find the transversal slice approximately corresponding to bregma + 0.5 mm. This position was used for subsequent ASL-MRI, which was based on a flow-sensitive alternating inversion recovery rapid acquisition with relaxation enhancement (FAIR-RARE) pulse sequence labeling the inflowing blood by global inversion of the equilibrium magnetization. One axial slice was acquired with a field of view of 15 × 15 mm, spatial resolution of 0.117 × 0.117 × 1 mm, TE of 5.368 ms, effective TE of 48.32 ms, recovery time of 10 s, and a RARE factor of 72. Twenty-two turbo inversion recovery values ranging from 30 to 2,300 ms were used, and the inversion slab thickness was 4 mm. The ASL images were analyzed by ImageJ and the average CBF value is reported in mL per 100 g of tissue per min.

Cell suspension preparation from lymph nodes, spleen and blood. At the indicated timepoints, mesenteric, axillary, inguinal, deep and superficial cervical lymph nodes were extracted, placed on a premoistened 70-μm cell strainer, gently

triturated, washed with 10 mL of PBS and spun at 500*g* for 7 min[34]. The cell suspension was then either stained for flow cytometry analysis or processed for analysis of intracellular cytokines. The spleen was removed, its epithelium was cut longitudinally and cells were isolated as described for the lymph nodes. Blood (150 μL) was drained from the submandibular venous plexus into heparinized tubes, incubated with erythrocytes lysis buffer and spun at 500*g* for7 min, and cells were stained for flow cytometry analysis[34].

Isolation of intestinal lamina propria mononuclear cells. Mice were killed by anesthesia overdose, and small and large intestines were removed and separated. Peyer patches were cut out from the small intestine and both small and large intestines were completely cleaned of mesenteric fat and intestinal contents[34]. Then intestines were opened longitudinally, washed of fecal contents with PBS, cut into approximately 1 cm pieces and placed into 20 mL of HBSS/10 mM HEPES, 8% FBS, 4 mM EDTA, 0.5 mM DTT. Next intestinal pieces were washed three times in a shaking incubator set at 250 rpm and at 37 °C for 20 min. After each round, intestinal pieces were vortexed for 20 s and the cell suspension containing intraepithelial lymphocytes (IELs) was collected. Suspensions from the three washes of IELs were combined and filtered over 0.3 g of prewashed nylon wool placed into a 10-mL syringe and then over a 70-μm strainer. Intestinal pieces were washed with complete PBS to remove EDTA, minced thoroughly with scissors and placed into 5 mL of 0.2 mg/mL of collagenase D in HBSS/10 mM HEPES with 5% of FBS. Then the intestinal pieces were digested at 250 rpm and 37 °C for 20 min, followed by 20 s of vortex[34]. The resulting cell suspension contained the LPMCs, and was filtered with a 40-μm nylon cell strainer; the strainer was washed with 10 mL of PBS. LPMCs cell suspensions were spun at 500*g* for 10 min at 4 °C. Cell pellets were resuspended in 8 mL 44% Percoll and overlaid on 5 mL of 67% Percoll. Gradients were centrifuged at 500*g* for 20 min at 4 °C (without brake) and cells at the interface were collected and washed with 10 mL of PBS. Cells were then spun at 500*g* for 10 min at 4 °C and cells were stained for flow cytometry analysis or used for in vitro stimulation.

Isolation of brain leukocytes. Isolation of brain leukocytes was performed as described[34]. Briefly, mice were anesthetized with pentobarbital and transcardially perfused with 20 mL cold PBS. Brains were removed, olfactory bulbs and cerebella excised, and hemispheres separated. Both hemispheres were placed in a dounce containing 3 mL RPMI-1640 medium (Sigma) with phenol red and gently homogenized. Then 4 mL of RPMI-1640 and 3 mL of 100% Percoll (final concentration 30% Percoll) were added and overlaid on 2 mL of 70% Percoll. Gradients were centrifuged at 500*g* for 30 min at 18 °C. Cells were recovered from the interface, washed twice with PBS, pooled (*n* = 2 mice/sample) and either stained for flow cytometric analysis or stimulated in vitro for analysis of IL-17.

Meningeal cell isolation. Mice were anesthetized with pentobarbital and transcardially perfused with 20 mL cold PBS. The upper portion of the skull was separated from the brain and the meninges were recovered from the interior of the skull bones, using a dissection microscope. Meninges were placed on the surface of a premoistened 70-μm cell strainer. Tissue was gently homogenized with the end of a 1-mL syringe plunger, washed with 10 mL PBS and centrifuged at 500*g* for 7 min. Cells were either stained for flow cytometric analysis or stimulated in vitro for analysis of IL-17.

Flow cytometry analysis. For surface marker analysis, 1×10^6 cells approximately were resuspended in 50 μL of FACS buffer (PBS with 2% FBS and 0.05% NaN_3). Cells were blocked with anti-CD16/CD32 for 10 min at 4 °C and then stained with the appropriate antibodies for 15 minutes at 4 °C. The following antibodies were used for extracellular staining: CD45 (clone 30F-11), CD4 (clone RM4-5), TCRβ (clone H57-597), TCRγδ (clone GL3), CD11b (clone M1/70), Ly6G (clone 1A8), CD11c (clone N418), NK1.1 (clone PK136) and CD19 (clone 6D5), all from Biolegend[34]. Cells were washed with FACS buffer, resuspended in 200 μL of FACS buffer and acquired in MACS Quant from Myltenyii Biotech. Analysis was performed with FlowJo. For intracellular staining, cells were first stained for extracellular markers as indicated above, and then fixed and permeabilized using fixation and permeabilization buffers from eBiosciences, following the manufacturer's instructions. Briefly, cells were fixed with fixation buffer for 30 min at 4 °C, washed with permeabilization buffer and incubated for 30 min with the appropriate antibodies in permeabilization buffer at 4 °C. The following antibodies were used for intracellular staining: FoxP3 (clone FJK-16s) and IL-17A (clone eBio17B7), both from eBiosciences. Finally cells were washed with permeabilization buffer and resuspended in FACS buffer, acquired in MACSQuant and analyzed with FlowJo[34]. Additionally, in other experiments endothelial cells (CD45lo/Ly6Chi) were sorted on a BD FACSAria II SORP (BD Bioscience) for mRNA analysis.

In vitro stimulation for intracellular IL-17 analysis. For IL-17 intracellular analysis, cells were isolated as indicated previously and resuspended in RPMI-1640 with 10% FBS and 100 ng/mL of PMA, 1 μg/mL of ionomycin. Brefeldin A (3 μg/mL) was added when wild-type mice were used. Cells were incubated for 4 h at 37 °C in the cell incubator, and then washed and stained as indicated previously for flow cytometry analysis[34]. Please see Supplementary Figure 15 for the flow cytometry gating strategy used for IL-17+ cells.

IL-17 detection. IL-17 concentration in plasma was measured by cytometric bead array mouse IL-17A Enhanced Sensitivity Flex Set, according to the manufacturer's instructions.

Novel object recognition test. The novel object recognition test (NOR) task was conducted under dim light in a plastic box measuring 29 cm × 47 cm × 30 cm high. Stimuli consisted of plastic objects that varied in color and shape but were similar in size[37]. A video camera mounted on the wall directly above the box was used to record the testing session for offline analysis. Mice were acclimated to the testing room and chamber for 1 d prior to testing (30 min in the testing room and 5 min to explore the empty box). Twenty-four hours after habituation, mice were placed in the same box in the presence of two identical sample objects and were allowed to explore for 5 min. After an intersession interval of 1 h, mice were placed in the same box, but one of the two objects was replaced by a novel object. Mice were allowed to explore for 5 min. Exploratory behavior was later assessed manually by an experimenter blinded to the treatment group. Exploration of an object was defined as the mouse sniffing the object or touching the object while looking at it. Placing the forepaws on the objects was considered as exploratory behavior, but climbing on the objects was not. A minimal exploration time for both objects (total exploration time) during the test phase (~10 s) was used. The amount of time taken to explore the novel object was expressed as percentage of the total exploration time and provides an index of recognition memory[37].

Barnes maze test. The Barnes maze consisted of a circular open surface (90 cm in diameter) elevated to 90 cm by four wooden legs[37]. There were 20 circular holes (5 cm in diameter) equally spaced around the perimeter, positioned 2.5 cm from the edge of the maze. No wall and no intramaze visual cues were placed around the edge. A wooden plastic escape box (11 × 6 × 5 cm) was positioned beneath one of the holes. Two neon lamps and a buzzer were used as aversive stimuli. The Any-Maze tracking system (Stoelting) was used to record the movement of the mice on the maze. Extramaze visual cues consisted of objects within the room (table, computer, sink, door, etc.) and the experimenter. Mice were tested in groups of seven to ten, and between trials they were placed into cages in a dark room adjacent to the test room for the intertrial interval (20–30 min). No habituation trial was performed. The acquisition phase consisted of three consecutive training days with three trials per day with the escape hole located at the same location across trials and days. On each trial a mouse was placed into a start tube located in the center of the maze, the start tube was raised, and the buzzer was turned on until the mouse entered the escape hole. After each trial, mice remained in the escape box for 60 s before being returned to their cage. Between trials the maze floor was cleaned with 10% ethanol in water to minimize olfactory cues. For each trial mice were given 3 min to locate the escape hole, after which they were guided to the escape hole or placed directly into the escape box if they failed to enter the escape hole. Four parameters of learning performance were recorded: (i) the latency to locate (primary latency) and (ii) enter the escape hole (total latency), (iii) the number of errors made and (iv) the distance traveled before locating the escape hole[37]. When a mouse dipped its head into a hole that did not provide escape was considered an error. On days 4 and 5, the location of the escape hole is moved 180° from its previous location (reverse learning) and two trials per day were performed.

Immunofluorescence. C57BL/6-IL-17a^tm1Bcgen/J mice were anesthetized with sodium pentobarbital (120 mg/kg, i.p.) and perfused transcardially with phosphate-buffered saline (PBS) followed by 4% paraformaldehyde (PFA) in PBS. Distal small intestine was removed, stored overnight in 4% PFA, and then submerged in 30% sucrose solution for 2 d. Sections (thickness: 30 μm) were cut through the whole distal small intestine using a cryostat and then place on a slide. Coronal sections were stained with nuclear marker ToPro-3 (1:2,000 in PBS) for 30 min. After washes, sections were visualized with both a confocal microscope (Leica TCS SP5) and an epifluorescence microscope (IX83 Inverted Microscope, Olympus).

qRT-PCR. Samples were collected in TRIzol (Invitrogen Life Technologies) and RNA was extracted according to the manufacturer's instructions. RNA samples were treated with Rnase free DnaseI (Roche) to remove DNA contamination. cDNA was produced from mRNA samples using the RevertAid First Strand cDNA Synthesis Kit (Thermo Scientific). Quantitative determination of gene expression was performed on a Chromo 4 Detector (Bio-Rad, Hercules, CA) using a two-step cycling protocol. Hypoxanthine-guanine phosphoribosyltransferase (HPRT) was used to normalize gene expression. qRT-PCR was conducted with cDNA in duplicate 15-μL reactions using the Maxima SYBR Green/ROX qPCR Master Mix (2X) (Thermo Scientific). The reactions were incubated at 50 °C for 2 min and then at 95 °C for 10 min. A polymerase chain reaction cycling protocol consisting of 15 s at 95 °C and 1 min at 60 °C for 45 cycles was used for quantification. Relative expression levels were calculated according to Livak and Schmittgen[34], and values were normalized to respective normal diet samples. Please see Supplementary Table 2 for the sequence of the primers used for qRT-PCR experiments.

Brain endothelial cell cultures. Immortalized murine (bEnd.3) and human (HBEC-5i) brain microvascular endothelial cells were obtained from ATCC and maintained in D-MEM supplemented with 10% (v/v) heat inactivated FBS, 100 units/mL penicillin, 100 μg/mL streptomycin and 4 mM L-glutamine[33]. Cells were

split 1:4 to 1:8 upon reaching confluence and cultured in six-well plates. Where indicated, cells were treated with rIL-17A (1–10 ng/mL; Peprotech) and Y27632 (5 μM; Tocris) for 24 h. At the end of the experiment, culture medium was removed, cells were washed twice with ice-cold PBS and lysed in RIPA buffer (100 μL)[33].

Nitric oxide measurement in bEnd.3 cells. For nitric oxide measurement, bEnd.3 cells were incubated with the NO-sensitive fluorescent dye DAF-FM (4-amino-5-methylamino-2′,7′-difluorescein) diacetate (5 μM; Molecular Probes) for 30 min and then rinsed for 30 min. DAF-FM is loaded into cells and is converted to DAF-2 by intracellular esterases, rendering it membrane impermeable. DAF-FM imaging was performed using an inverted fluorescence microscope (Nikon) equipped with a CCD camera (Princeton Instruments). Time-resolved fluorescence was measured every 30 s with an exposure time of 200 ms using image analysis software (IPLab, Scanalytics Inc). After a stable fluorescence baseline was achieved, cells were superfused with oxygenated D-MEM in the presence of rIL-17A (10 ng/mL; Peprotech) and NO production was induced by adding ACh (100 μM). In some experiments, cells were also treated with the ROCK inhibitor Y27632 (5 μM; Tocris), the p44/42 MAPK inhibitor PD98059 (10 μM; Tocris) or the PKC inhibitor Go6976 (1 μM; Tocris). Time-control experiments in which rIL-17A was not superfused were performed in parallel to assure the stability of the preparation.

Nitric oxide measurement in pial microvessels. Pial microvessels were removed under a dissecting microscope[50] and incubated with DAF-FM (25 μM; Molecular Probes) in L-ACSF at room temperature for 45 min[24,50]. Time-resolved fluorescence was measured every 60 s with an exposure time of 150 ms using image analysis software (IPLab, Scanalytics Inc). After a stable fluorescence baseline was achieved, microvessels were superfused with ACh (100 μM) for 15 min. In some experiments, prior to ACh administration, microvessels were pretreated with a DAF-FM solution containing L-arginine (5 mM). DAF-FM fluorescence intensity is expressed as RFU/μm², where RFU is the relative fluorescence unit, and μm² is unit of the area in which RFU was measured.

Western blotting. Cerebral blood vessels and brain microvascular endothelial cells samples were lysed in RIPA buffer (50 mM Tris-HCl pH 8.0, 150 mM NaCl, 0.5% deoxycholic acid, 0.1% SDS, 1 mM EDTA pH 8.0, 1% IGEPAL CA-630) and equal volumes were mixed with SDS sample buffer, boiled, and analyzed on 4–12% SDS polyacrylamide gels. Proteins were transferred to PVDF membranes (Millipore), blocked with 5% milk in TBS/0.1% Tween-20 (TBST) and incubated with polyclonal anti-phospho-eNOS (Ser[1177]), anti-phospho-eNOS (Thr[495]) and anti-eNOS (1:1,000, Cell Signaling cat. #9571, 9574 and 9572, respectively). Membranes were washed in TBST, incubated with goat anti-rabbit secondary antibodies conjugated to horseradish peroxidase (Santa Cruz Biotechnology), and protein bands were visualized with Super Signal West Femto Maximum Sensitivity Substrate (Thermo Fisher Scientific) or Clarity Western ECL Substrate (Bio-Rad) on a Bio-Rad ChemiDoc MP Imaging System[33].

Blood–brain barrier permeability measurement. BBB permeability was assessed using fluorescein-dextran (FITC-dextran, MW = 3 kDa; 100 μL of 1% solution i.v.) as previously described[37]. The marker was allowed to circulate for 20 min, and then mice were transcardially perfused with ice-cold PBS. Brains were removed and brainstem and cerebellum were discarded. Samples were weighed and frozen on dry ice and stored at −80 °C. Tissue was homogenized with a sonicator in 400 μL of PBS and then mixed with 400 μL of methanol. After centrifugation, the amount of FITC-dextran (485-nm excitation and 530-nm emission) in the supernatant for each sample was determined in duplicate using a fluorescence spectrophotometer. Standard curves were obtained using 0–125 ng/mL of FITC-dextran. The values were normalized for the weight difference by dividing each sample value by the respective weight.

Statistics. Sample size was determined according to a power analysis based on previously published works published by our lab on CBF regulation. No animals were excluded. Mouse randomization was based on the random number generator function (RANDBETWEEN) in Microsoft Excel. Analysis was performed in a blinded fashion. GraphPad Prism (v. 6.0) was used for statistical analysis. Intergroup differences were analyzed by unpaired Student's t tests for single comparisons or by one- or two-way ANOVA (with Tukey's or Bonferroni's post hoc analysis tests) for multiple comparisons, as appropriate and indicated in the figure legends. Data distribution was assumed to be normal, but this was not formally tested. When variances were different, Welch's correction for unequal variances was applied to the t test results. Data are expressed as mean ± s.e.m. and differences were considered statistically significant at $P < 0.05$.

Life Sciences Reporting Summary. Further information on experimental design is available in the Life Sciences Reporting Summary.

Data availability. All data generated or analyzed during this study are included in this published article (and its supplementary information files).

References

50. Park, L. et al. Scavenger receptor CD36 is essential for the cerebrovascular oxidative stress and neurovascular dysfunction induced by amyloid-beta. *Proc. Natl. Acad. Sci. USA* **108**, 5063–5068 (2011).

nature research

Corresponding author(s): Costantino Iadecola

☐ Initial submission ☐ Revised version ☒ Final submission

Life Sciences Reporting Summary

Nature Research wishes to improve the reproducibility of the work that we publish. This form is intended for publication with all accepted life science papers and provides structure for consistency and transparency in reporting. Every life science submission will use this form; some list items might not apply to an individual manuscript, but all fields must be completed for clarity.

For further information on the points included in this form, see Reporting Life Sciences Research. For further information on Nature Research policies, including our data availability policy, see Authors & Referees and the Editorial Policy Checklist.

▶ Experimental design

1. **Sample size**

   Describe how sample size was determined.

   > Sample size was determined according to power analysis based on previous published works published by our lab on CBF regulation.

2. **Data exclusions**

   Describe any data exclusions.

   > No data were excluded.

3. **Replication**

   Describe whether the experimental findings were reliably reproduced.

   > All attempts at replication were successful.

4. **Randomization**

   Describe how samples/organisms/participants were allocated into experimental groups.

   > Mouse randomization was based on the random number generator function (RANDBETWEEN) in Microsoft Excel software.

5. **Blinding**

   Describe whether the investigators were blinded to group allocation during data collection and/or analysis.

   > Analysis was performed in a blinded fashion.

   Note: all studies involving animals and/or human research participants must disclose whether blinding and randomization were used.

6. **Statistical parameters**

   For all figures and tables that use statistical methods, confirm that the following items are present in relevant figure legends (or in the Methods section if additional space is needed).

n/a	Confirmed	
☐	☒	The exact sample size (n) for each experimental group/condition, given as a discrete number and unit of measurement (animals, litters, cultures, etc.)
☐	☒	A description of how samples were collected, noting whether measurements were taken from distinct samples or whether the same sample was measured repeatedly
☐	☒	A statement indicating how many times each experiment was replicated
☐	☒	The statistical test(s) used and whether they are one- or two-sided (note: only common tests should be described solely by name; more complex techniques should be described in the Methods section)
☐	☒	A description of any assumptions or corrections, such as an adjustment for multiple comparisons
☐	☒	The test results (e.g. P values) given as exact values whenever possible and with confidence intervals noted
☐	☒	A clear description of statistics including central tendency (e.g. median, mean) and variation (e.g. standard deviation, interquartile range)
☐	☒	Clearly defined error bars

   See the web collection on statistics for biologists for further resources and guidance.

▶ Software

7. Software

Describe the software used to analyze the data in this study.

Perimed and PowerLab were used for CBF measurements and MAP recording. FlowJo was used for analysis of flow cytometry experiments. Any Maze was used for collecting and analyzing behavioral experiments. Biorad Chemi Doc and Image Studio Ver 3.1 were used for collecting and analyzing immunoblots. Image J was used for analysis of ASL MRI data. IPLab was used for measurement of DAF fluorescence in experiments evaluating NO production in microvessels preparations or brain endothelial cell cultures. Graph Pad (v. 6.0) software was used for statistical analysis. Microsoft Excel was used for mouse randomization.

For manuscripts utilizing custom algorithms or software that are central to the paper but not yet described in the published literature, software must be made available to editors and reviewers upon request. We strongly encourage code deposition in a community repository (e.g. GitHub). *Nature Methods* guidance for providing algorithms and software for publication provides further information on this topic.

▶ Materials and reagents

8. Materials availability

Indicate whether there are restrictions on availability of unique materials or if these materials are only available for distribution by a for-profit company.

All materials are from standard commercial sources specified in the Methods section.

9. Antibodies

Describe the antibodies used and how they were validated for use in the system under study (i.e. assay and species).

The following commercial antibodies were injected in mice: Anti-IL-17A (Clone 17F3; bioXcell) and mouse IgG1 isotype control (Clone MOPC-21; bioXcell).
The following commercial antibodies were used in flow cytometry experiments: CD45 (clone 30F-11), CD4 (clone RM4-5), TCRβ (clone H57-597), TCRγδ (clone GL3), CD11b (clone M1/70), Ly6G (clone 1A8), CD11c (clone N418), NK1.1 (clone PK136), CD19 (clone 6D5) from Biolegend and FoxP3 (clone FJK-16s) and IL-17A (clone eBio17B7) from eBiosciences.
Anti-phospho-eNOS (Ser1177, #9571), anti-phospho-eNOS (Thr495, #9574) and anti-eNOS (#9572) from Cell Signaling were used to evaluate eNOS phosphorylation in microvessels preparations and brain microvascular endothelial cells. The antibodies used for western blotting experiments were validated in mice lacking eNOS.

10. Eukaryotic cell lines

a. State the source of each eukaryotic cell line used.

Immortalized brain mouse (bEnd.3) and human (HBEC-5i) brain endothelial cells were purchased from ATCC.

b. Describe the method of cell line authentication used.

The cell lines used in the study have been previously authenticated (please see www.atcc.org).

c. Report whether the cell lines were tested for mycoplasma contamination.

Cell lines were not tested for mycoplasma contamination.

d. If any of the cell lines used are listed in the database of commonly misidentified cell lines maintained by ICLAC, provide a scientific rationale for their use.

No commonly misidentified cell lines were used.

▶ Animals and human research participants

11. Description of research animals

Provide details on animals and/or animal-derived materials used in the study.

The following mouse strains were used in the study: C57BL/6 (JAX), B6.129S7-Rag1tm1Mom/J (RAG1-/-, JAX Stock #002216), IL-17atm1.1(icre)Stck/J (IL-17-/-, JAX Stock #016869) and C57BL/6-IL-17atm1Bcgen/J (IL-17GFP, JAX Stock #018472). Only male mice were used in this study.

12. Description of human research participants

Describe the covariate-relevant population
characteristics of the human research participants.

The study did not involve human participants.

nature research

Corresponding author(s):   Costantino Iadecola

☐ Initial submission   ☒ Revised version   ☐ Final submission

Flow Cytometry Reporting Summary

Form fields will expand as needed. Please do not leave fields blank.

▶ Data presentation

For all flow cytometry data, confirm that:

☒ 1. The axis labels state the marker and fluorochrome used (e.g. CD4-FITC).

☒ 2. The axis scales are clearly visible. Include numbers along axes only for bottom left plot of group (a 'group' is an analysis of identical markers).

☒ 3. All plots are contour plots with outliers or pseudocolor plots.

☒ 4. A numerical value for number of cells or percentage (with statistics) is provided.

▶ Methodological details

5.	Describe the sample preparation.	Please see manuscript page 19 to 22
6.	Identify the instrument used for data collection.	MACSQuant Analyzer
7.	Describe the software used to collect and analyze the flow cytometry data.	FlowJo
8.	Describe the abundance of the relevant cell populations within post-sort fractions.	5000 endothelial cells were collected by cell-sorting and used for qRT-PCR.
9.	Describe the gating strategy used.	Gating strategy is specified in the new supplemental figure. Gates were validated by TO-PRO-3 and fluorescein-diacetate labeling to identify dead and live cells, respectively. Isotype controls, single antibody-stained samples and Fluorescence Minus One controls were used to establish compensation and gating parameters.Samples were acquired and analyzed by an investigator blinded to the treatment groups.

Tick this box to confirm that a figure exemplifying the gating strategy is provided in the Supplementary Information. ☒

nature research

Corresponding Author: Iadecola Costantino

Date: 11/29/2017

Reporting Summary for MRI studies

Form fields will expand as needed. Please do not leave fields blank.

▶ Experimental design

1. Describe the experimental design.

Resting cerebral blood flow (CBF)

2. Specify the number of blocks, trials or experimental units per session and/or subject, and specify the length of each trial or block (if trials are blocked) and interval between trials.

n/a

3. Describe how behavioral performance was measured.

n/a

▶ Acquisition

4. Imaging

   a. Specify the type(s) of imaging.

   Arterial Spin Labeling MRI

   b. Specify the field strength (in Tesla).

   7.0 Tesla 70/30 Bruker Biospec small-animal MRI system with 450 mT/m gradient amplitude and a 4500 T · m−1 · s−1 slew rate

   c. Provide the essential sequence imaging parameters.

   ASL-MRI was based on a flow-sensitive alternating inversion recovery rapid acquisition with relaxation enhancement (FAIR-RARE) pulse sequence labeling the inflowing blood by global inversion of the equilibrium magnetization.

   d. For diffusion MRI, provide full detail on imaging parameters.

   n/a

5. State area of acquisition

The resting cerebral blood flow was measured in the cortex and in the hippocampus.

▶ Preprocessing

6. Describe the software used for preprocessing.

Provide detail on software version and revision number, and on specific parameters (model/functions, brain extraction, segmentation, smoothing kernel size, etc.)

7. Normalization

   a. If data were normalized/standardized, describe the approach(es).

   Specify linear or non-linear and define image types used for transformation.

   b. Describe the template used for normalization/transformation.

   Specify subject space or group standardized space (e.g. original Talairach, MNI305, ICBM152).

8. Describe your procedure for artifact and structured noise removal.

Specify motion parameters, tissue signals and physiological signals (heart rate, respiration).

9. Define your software and/or method and criteria for volume censoring and state the extent of such censoring.

▶ Statistical modeling & inference

10. Define your model type and settings.

Specify type (mass univariate, multivariate, RSA, predictive, etc.) and describe essential details of the model at the first and second levels (e.g. fixed, random or mixed effects; drift or auto-correlation).

11. Specify the precise effect tested.

We tested the effect of high salt diet on the resting CBF

12. Analysis

a. Specify whether analysis is whole brain or ROI-based.

The analysis id ROI-based

b. If ROI-based, describe how anatomical locations were determined.

The resting CBF was measured in the cortex and in the hippocampus

13. State the statistic type for inference. (See Eklund et al. 2016.)

The images were analzyed by Image J and the average CBF value is reported as mL per 100g of tissue per minute.

14. Describe the type of correction and how it is obtained for multiple comparisons.

Data were analyzed by One-way ANOVA plus Tukey's test for multiple comparisons.

15. Connectivity

a. For functional and/or effective connectivity, report the measures of dependence used and the model details.

n/a

b. For graph analysis, report the dependent variable and functional connectivity measure.

n/a

16. For multivariate modeling and predictive analysis, specify independent variables, features extraction and dimension reduction, model, training and evaluation metrics.

n/a